INKJET PRINTED FLEXIBLE PATCH ANTENNAS FOR FULL DUPLEX AND CIRCULAR POLARIZATION APPLICATIONS

By

ABDUL RAKIB HOSSAIN

A thesis submitted in partial fulfillment of
the requirements for the degree of

MASTER OF SCIENCE IN ELECTRICAL ENGINEERING

WASHINGTON STATE UNIVERSITY
School of Engineering and Computer Science, Vancouver

DECEMBER 2022

To the Faculty of Washington State University:

The members of the Committee appointed to examine the thesis of ABDUL RAKIB HOSSAIN find it satisfactory and recommend that it be accepted.

_____

Tutku Karacolak, Ph.D., Chair

_____

Praveen Sekhar, Ph.D.

_____

Feng Zhao, Ph.D.

ACKNOWLEDGMENT

I would like to express my deepest gratitude to my advisor Dr. Tutku Karacolak for his guidance, advice, mentoring, and most importantly, his constant pushing and motivation toward my research work. His words also helped me to choose the next destination of my academic journey. I would also like to thank Dr. Praveen Sekhar for being my committee member and for providing me with his lab support for my thesis work. I am also thankful to Dr. Feng Zhao for being my committee member and providing guidance for literature reviewing.

My current and past lab members, Tuan Nguyen, Md. Rabiul Hasan, and Aleks Mertvyy for their support and advice. I am specially thankful to my lab alumni Gregory Makar and his current workplace, Pulse Larsen Antennas for providing me anechoic chamber facility for some of my antenna measurements. I am also grateful to Dr. Sekhar's lab members, Sharadindu Gopal Kirtania, Md Samiul Islam Sagar, and Bachir Younes for supporting me with the inkjet printing.

I like to thank my roommate Md. Sadiqul Islam and Abdulla Al Mamun, for whom I never felt alone even when I am eight thousand miles away from home. I am grateful to ISI, my friendship family, Tyler, and Lydia, for making my life easier and helping me settle down. WSUV Bangladeshi community also helped me in this two years journey and cheered me up when I was down and needed motivation.

Finally, I thank my parents and younger brother for always being my hope and source of inspiration. I am indebted to them for providing me with support throughout my whole academic life.

INKJET PRINTED FLEXIBLE PATCH ANTENNAS FOR FULL DUPLEX AND CIRCULAR POLARIZATION APPLICATIONS

Abstract

by Abdul Rakib Hossain, M.S.
Washington State University
December 2022

Chair: Tutku Karacolak

Flexible devices are getting more popular nowadays because of it's lightweight, small size, portability, less expensive, environment friendly, and disposability. Flexible antenna, part of flexible devices, has become an important component of research for electrical engineers. The flexible antenna can be built using different materials like PET, PEN, liquid crystal polymer, PDMS, and textiles like woolen felt, cotton, cordura, and fleece as substrate. This thesis focuses on designing and fabricating antennas on PET paper by using inkjet printing for full duplex and circular polarization applications. Firstly, a flexible full duplex antenna is proposed with robust performance and high isolation for 5.8 GHz using foam and PET paper. The patch of the antenna is modified by corner cut and inset feeding, while the defected ground structure is used to improve isolation between transmit and receive ports. Silver nanoparticle ink is used for printing the antenna in an inkjet printer. The fabricated version supports simulated results by showing acceptable performance in desired bandwidth. Bending tests and human body loading experiments are carried out on the fabricated antenna to demonstrate the antenna's effectiveness for wearable applications. To the best of author's knowledge, this is the first flexible full duplex antenna

designed, achieving a high isolation level of -50 dB. Moreover, wide bandwidth, improved gain, and radiation efficiency, low cost, easy fabrication, and robust performance make it a good option for 5.8 GHz wearable applications. Secondly, a simple and compact CPW-fed circularly polarized antenna is presented. The proposed antenna consists of a modified “S” shaped patch, which has slots in three different places along with a slot in the ground plane. These slots contribute to increasing the bandwidth of the axial ratio. The antenna has a 3 dB axial ratio bandwidth of 10.47% (4.07 GHz- 4.52 GHz) and an impedance bandwidth of 17.53% (3.8 GHz - 4.53 GHz) covering the full region of axial ratio band. Moreover, this antenna is designed using PET paper which makes it flexible in nature and the first flexible antenna in the discussed frequency range to the best of author’s knowledge. Finally, an inkjet printed circularly polarized antenna using CPW feeding on PET substrate is proposed. The antenna is designed and optimized using ANSYS HFSS, which operates at 4.01 GHz - 5.05 GHz and 6.23 GHz - 7.58 GHz with a return loss of < -10 dB. On top of that, the antenna shows an axial ratio of less than 3 dB at 4.23 GHz - 4.62 GHz and 7.11 GHz - 7.36 GHz, whereas left hand circular polarization (LHCP) is observed in the first band and right hand circular polarization (RHCP) is observed in the second band. The dimension of the antenna is 31 mm x 37 mm x 0.135 mm. Measurement of the fabricated version shows good agreement with the simulated version. To the best of author’s knowledge, this antenna is the first flexible CPW-fed circularly polarized antenna with dual band.

TABLE OF CONTENTS

Page

LIST OF TABLES

Page

LIST OF FIGURES

Page

Dedication

I dedicate this thesis to my parents, Md Elias Hossain and Rezia Begum,

and my younger brother, Abdul Hasib Hasan Zayed,

for being my source of motivation

and energy.

CHAPTER ONE: INTRODUCTION

Flexible Antennas:

With the ongoing “Fourth Industrial Revolution” and “5G era”, human is getting more and more dependent on technologies for their day-to-day life. For education, entertainment, health care, connectivity, agriculture, business, and every other sector, internet of things (IOT) devices play major roles in improving the lifestyle. To keep up with this fast pace of technological transformation, engineers are solving complex problems every day. One of which is creating devices to connect everyone with the fast speed of the internet 5G is offering. As a result, it has become inevident to develop cheap, lightweight, portable, environment-friendly, and disposable devices using flexible electronics. To connect these devices to the internet, integration of flexible antenna system is a must. Primarily, flexible antennas have to have good tolerance of mechanical deformation, be susceptible to miniaturization, and be endurance to the external environment. Different metal nanoparticles, conductive polymers, graphene-based materials, and liquid metal can be used as the conductor for fabricating the antenna. For substrate, PET, PEN, polyimide, PDMS, LCP, and different textile materials can be used. The main task is to fabricate the antenna using the substrate and the conductive element, which can be done by using inkjet printing, screen printing, 3D printing, chemical etching, substrate-integrated waveguide technology, and stitching and embroidery for textile antennas, etc. Biocompatible polymer substrates also allow antennas to be used for implantable and ingestible applications. For both cases, a low specific absorption rate (SAR) is necessary to protect the human body from the effect of electromagnetic radiation. Ingestible antennas are mainly used for drug delivery and monitoring the internal conditions of the patient, which are considered a special type of flexible antennas.

Full duplex technology and self-interference issue:

As discussed in the previous section, frequency spectrums are getting highly crowded because of the increased number of devices connected to the internet every day. In the existing wireless systems, data are transferred using semi duplex mode by either time division multiplexing or frequency division multiplexing. Full duplex system, where data will be transmitted and received at the same frequency and at the same time, can be a lucrative option to counter spectrum congestion. Full duplex technology theoretically doubles the spectrum efficiency as the transmitter and receiver will use the same slot [1]. Additionally, full duplex has higher throughput and reduced outrage probability than half duplex mode [2].

Though full duplex mode is more efficient than current technology, widespread implementation is not seen in modern wireless devices. The main reason that is limiting the potential of the full duplex system is the effect known as self-interference. Self-interference refers to the interference that is created by the transmitter to its own receiver end. It is known that wifi signals are transmitted at 20 dBm, and the receiver noise floor is -90 dBm. So, the transmission signal has to be canceled by 20 dBm -(-90 dBm) = 110 dBm to make it negligible for interference in the receiver signal. Any cancellation smaller than this amount will act as noise and reduce the SNR in the received signal [3]. This cancellation is made in three steps: Propagation domain, analog circuit domain, and digital domain. Propagation domain falls in passive mitigation scheme, whereas analog circuit domain and digital domain fall in active mitigation scheme. In propagation domain, cancellation is mainly done by the properties of antennas like path loss, cross-polarization, and antenna directionality. As cancellation using antennas is the topic of interest of this thesis, a through study will be done later in this section with a literature review. Analog circuit domain

cancellation happens right before the signal enters analog-to-digital converter (ADC). The advantages of cancellation in the analog circuit domain are easy implementation, low complexity, advanced optimization, reduced power of residual SI, adapting varying signal to noise ratios. The final step for self-interference cancellation is using advanced DSP techniques to the received signal. Digital cancellation is easier because it doesn't contain any circuit complexity and power consumption. However, digital cancellation methods require a large amount of SI cancellation before the signal enters to ADC. This leaves the antenna and analog circuits to complete a significant amount of cancellation before the digital cancellation. Figure 1.1 shows some methods of self-interference cancellation under different schemes.

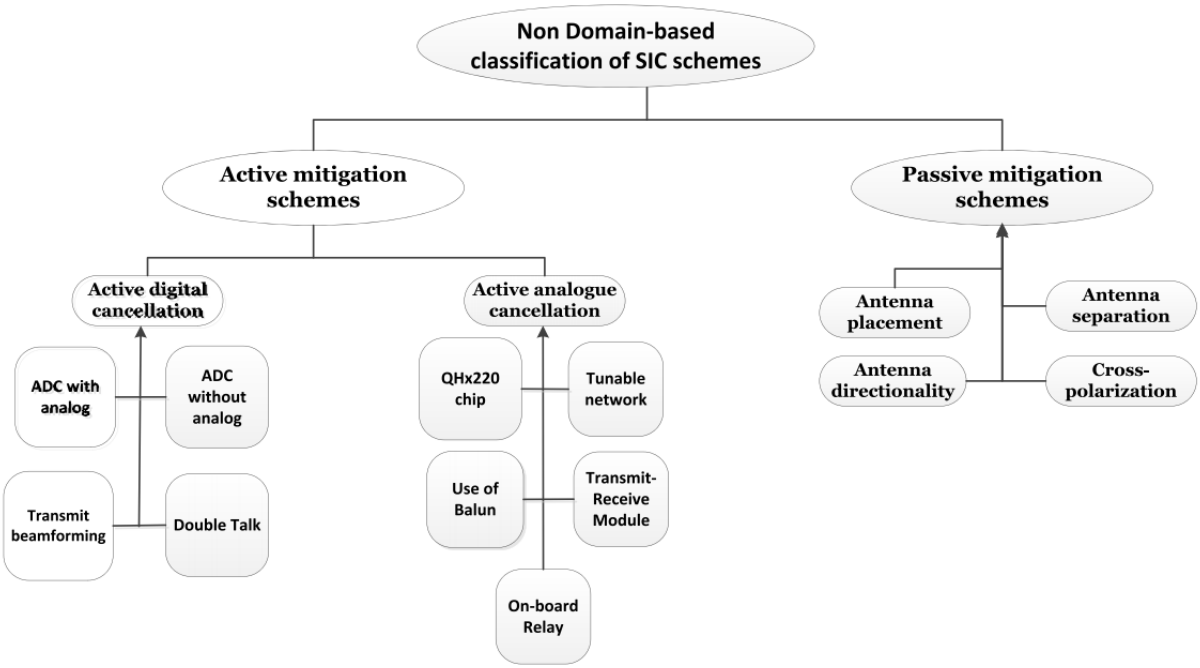

Figure 1.1: Self-interference cancellation methods [4].

Full duplex antenna architecture review:

As discussed earlier, antenna architecture plays a significant role in achieving a targeted amount of self-interference cancellation. -50 dB isolation between the antenna's TX and RX port is considered reasonable to further process the interference level in the analog circuit and digital domain. S21 parameter represents this isolation amount in a full duplex antenna. S21 simply means the amount of power transferred from port 1 to port 2. For example, S21 = -20 dB indicates that if 1 W is transmitted through port 1, 10^{-2} W will be received in port 2. A number of techniques is proposed for attaining high isolation value in the shared antenna structure. However, most of these antennas are on rigid substrates like FR4, Rogers, RT/duroid, taconix etc. Antennas are proposed from 1 GHz to 18 GHz frequency with isolation of -20 dB to -90 dB through various techniques.

Orthogonal polarization:

In orthogonal polarization, transmission and receiver ports are fed by placing them in 90^{o} angle with each other. In [5], a single orthogonally polarized antenna system connected with two RF couplers, attenuators, and voltage variable phase shifter was proposed for 1.014 GHz - 1.036 GHz with 40 dB isolation on FR4 material. Douglas et al. [6] proposed three configurations of U-slotted patch antenna using orthogonal polarization and symmetrical cancellation of the radiated field. This antenna works at 1.7 GHz- 2.2 GHz with isolation of around 30 dB.

Integrated antenna technique:

In this method, isolation is done by attaching different types of circuit elements like coupler, power divider, voltage phase shifter, and attenuator etc., along with the patch. Li et al. [7] proposed a dual band dual-polarized antenna (DBDP) antenna Digital Cellular System (DCS) and Wideband Code Division Multiple Access (WCDMA) band where the back side of the ground plane contained four groups of the split ring resonator, and the front side of the ground plane

contained an H-shaped and a U-shaped slot. These slots fed energy to the radiation patch in the top layer. A piece of foam was used in the space between the top and ground layers. This antenna has dual bandwidth working from 1.72 GHz - 1.88 GHz and 1.92 GHz – 2.17 GHz with an isolation of 21 dB and 35 dB, respectively. In [8], a power distributing duplex network (PDDN) that offers port isolation was introduced in a 2 x 1 antenna array with 35 dB isolation. Nawaz et al. [9] attached two 15 dB couplers, voltage-controlled phase shifters, and attenuator in the presentation of a compact, monostatic slot coupled antenna which works at 2.44 GHz - 2.46 GHz and 2.48 – 2.5 GHz. In [10], a full duplex system was proposed combining a 180°directional coupler with three patch antennas where one was used as a receiver, and the other two were used as transmitters. Transmitters were fed a 180° phase difference signal with equal amplitude to ensure high cancellation of around 50 dB. Nawaz et al. [11] proposed a dual-polarized proximity-fed patch antenna integrated with a single tap self-interference cancellation (SIC) circuit, which consisted of 10 dB coupler in each port, a variable phase shifter, and a tunable attenuator. After that, another design of two-taps SIC circuit was proposed while the second tap contained a phase shifter and attenuator so that each single from TX and RX port can use separate SIC circuit. Chaudhary et al. [12] proposed a phase reconfigurable feeding network consisted of voltage control varactor diodes and a power dividing circuit which used to excite the TX radiating patch while a single ended co-axial feeding network was used to excite RX patch. Both patches were circular in shape showing a high isolation of 65 dB.

Antenna array:

The array of patches is used for creating different polarized radiation patterns resulting in a good amount of isolation between ports. Laco et al. [13] proposed a patch antenna array where transmitters and receivers were placed opposite each other. A rat race coupler was used to feed the

transmitter antenna to create a 180° phase difference between two transmitter ports. Positions of ports were carefully determined to maximize cross-polarization coupling in the 2.4 GHz – 2.5 GHz range. The antenna array is particularly useful for designing C-band antennas which are particularly useful for satellite communication. In [14], a 2x2 antenna array was proposed using the parasitic patch, air gap with compact slotline-based balun, and power divider as a feeding network. After that, a 4x4 antenna array where the 2x2 antenna array was used as a subarray which provides an isolation of 65 dB which works in 4.5 GHz - 5.8 GHz. A corporate feeding network (CFN) with a pairwise antiphase feeding technique was used in [15], which was proposed for applications in U-NII 5.15-5.925 frequency band. Parasitic patches were also used here for extending the frequency band in this four-element antenna array. In [16], an array of 2 patches and a single patch with 4 ports was proposed. Another 1x4 antenna array was proposed with a compact slotline-based 180° hybrid feeding system consisting of common mode feeding and differential mode feeding with rat race topology [17]. Douglas et al. [18] proposed a U-slot patch antenna excited by a coaxial probe fed and then created a square grid configuration using 4 patch antennas fed by a wideband hybrid coupler. This antenna has a high bandwidth of 1.7 GHz working from 5.24 GHz – 6.94 GHz with an isolation of 52.3 dB. In [19], a modified version of the franklin patch antenna was proposed, which incorporated 12 patches separated by phase-shifting non-radiating structures. This antenna can generate either right-hand circularly polarized (RHCP) waves or left-hand circularly polarized (LHCP) waves with high inter-port isolation making it fit for polarimetry and satellite applications. Zhang et al. [20] proposed a 8 x 8 dual-polarized antenna array with square patch elements where orthogonal polarization was induced in TX and RX patches. Slotline-based baluns and lumped resistors were employed for differential feeding and improvement of

impedance performance and radiation efficiency, respectively. This antenna works at a much higher frequency (13.6 GHz – 15.7 GHz) with a very high gain of 22.4 dB.

Ring hybrid structure:

In a ring hybrid structure, four ports are constructed with a distance of $\frac{\lambda}{4}$ between each adjacent port which is shown in Figure 1.2. This structure is frequency-specific structure.

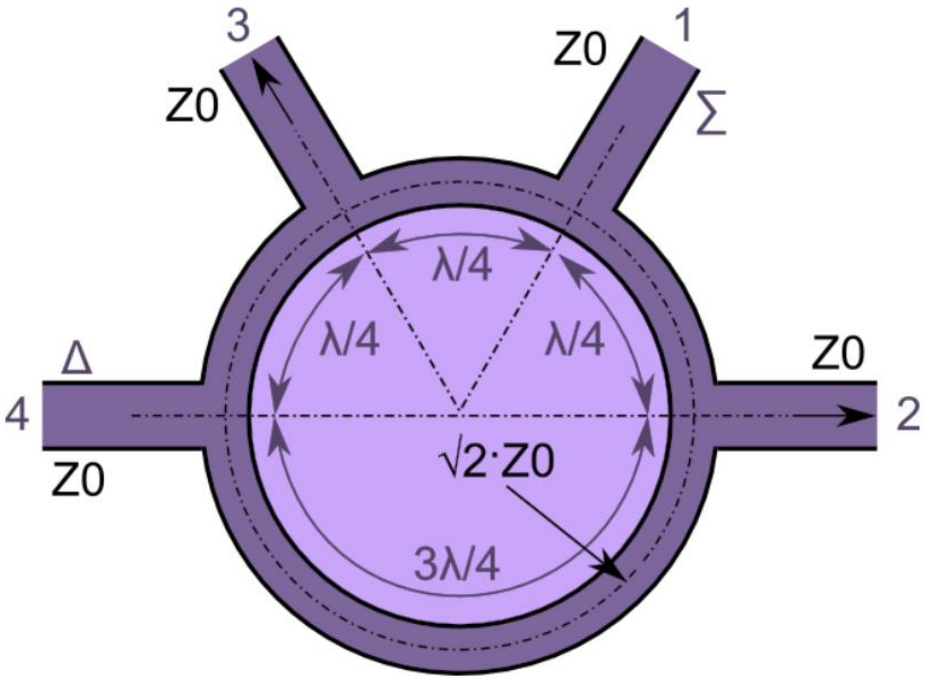

Figure 1.2: Ring hybrid structure [21].

Port 4 works here as a different port, while port 1 works as a summation port. Input in port 4 will be divided in 180^{o} out of phase in port 3 and port 2, which will ultimately cancel each other. Input in port 1 will be divided in equal half between port 2 and port 3 in the same phase. Ring hybrid is primarily used for constructing antennas in S band. In [22], two dual-polarized differential fed three port antenna was proposed. Differential feeding was done by ring hybrid structure in 2 RX ports. For the first antenna TX port was a microstrip feed line, while for the

second antenna TX port was aperture coupled. Another three-port antenna with proximity coupling was proposed by Nawaz et al. [23] where antenna characteristics for linear co-polarization and dual polarization were investigated. In another proposal, Nawaz et al. [24] used double differential feeding, meaning ring hybrid coupler for both TX and RX ports in a 4 port patch antenna. A 180° ring hybrid structure was proposed for WLAN using probe fed, and aperture-fed systems [25]. A comparison of properties was also discussed, along with the fabrication procedure. In [26] sum port of the ring hybrid structure was removed and used while designing a probe-fed patch antenna. Nawaz et al. [27] used a ring hybrid structure in the receiver port while proposing a single patch antenna in a single layer with three microstrip-T (MS-T) feeds using DC isolated ports. Khaledian et al. [28] provided a robust SIC technique using a double-stack rectangular patch antenna with a phase reconfigurable rat race circuit in the receiver port to increase the operational bandwidth. Phase reconfiguration was done by a low-loss varactor diode connected in series with the rat race circuit. Nawaz et al. [29] proposed another antenna that was bistatic in nature and had small form factor using two closely spaced rectangular patches with a ring hybrid coupler for differential feeding. Nawaz et al. [30] proposed another antenna system where a ring hybrid structure was used for differential feeding a 1x2 antenna array. Lu et al. [31] proposed an antenna with rat-race coupler and four micro-strip patches for radar sensing applications. This antenna works at 5.8 GHz with an isolation of 35 dB. In [32], two 3-port ring hybrid couplers were used with four feeding probes in the bottom substrate, and four meticulously designed patches were used in the top substrate to cover 90% of the bandwidth of the fixed satellite band. This antenna works in a much higher frequency, like 11.6 GHz – 12.2 GHz, with an isolation of 70 dB.

Defected ground structure:

Defected ground structure (DGS) is developed based on photonic band gap (PBG) structures or electromagnetic band gap (EBG) structures. DGS basically cut the ground plane in different shapes, creating a disturbance in the shield current distribution. Eventually, the size and placement of the DGS increase the path length of the surface current, which results in the attenuation of signals and suppressing noise. Some full duplex antennas are proposed in S-band using DGS. In [33], a dual port patch antenna with "H" shaped defected ground beneath the feedline was proposed. In [34], a three layer antenna with DGS in the middle layer was proposed. Five dumbbell lattice defects were optimum, providing less than -60 dB isolation. Another 4 port rectangular patch with rectangular shape DGS with differential feeding done by two identical branch-line baluns was proposed in [35]. Hussein et al. [36] proposed an antenna with gear shaped radiating patch and two omega shaped DGS structures beneath the feeding line. DGS structure was used as a bandpass filter (BPF) where the resonant frequency of BPF was controlled by appropriate scaling of the DGS. In [37], the author proposed a hybrid integration of "dumb-bell" shape Uniplanar EBG(UC-EBG) and DGS to realize low mutual coupling on the basis of band-stop filtering phenomenon in the center frequency of the bandwidth in a four element linear array patch antenna. This antenna is implemented on FR4 with a 30 dB isolation at 5.8 GHz.

Circularly polarized antenna:

Gain is an important parameter to consider to improve the system's performance. For linearly polarized antennas, where two orthogonal components are in the same phase or 180^{o} out of phase polarization loss factor reduces the efficiency and the gain of the antenna. Also, for mobile or portable devices, it is difficult to increase polarization matching to reduce the loss factor.

Circularly polarized antenna increases the gain of the antennas as it makes the polarization loss factor 0 theoretically.

To understand circular polarization, let's say an electric field is traveling in negative z direction. x and y components can be written as below:

$$E_x(z,t) = E_{x0}\cos(\omega t + kz + \Phi_x) \quad (1)$$

$$E_y(z,t) = E_{y0}\cos(\omega t + kz + \Phi_y) \quad (2)$$

For circular polarization, the magnitudes of these two components have to be the same and phase difference has to be the odd multiple of $\frac{\pi}{2}$.

$$E_{x0} = E_{y0} \quad (3)$$

$$\Delta\Phi = \Phi_y - \Phi_x = \begin{cases} +\left(\frac{1}{2}+2n\right)\pi, n = 0,1,2 \ldots & for\ CW \\ -\left(\frac{1}{2}+2n\right)\pi, n = 0,1,2 \ldots & for\ CCW \end{cases} \quad (4)$$

where CW stands for clockwise and CCW stands for counterclockwise. Clockwise and counterclockwise rotation is regarded as right-hand circular polarization and left-hand circular polarization, respectively.

The parameter to determine polarization is the axial ratio (AR). For a perfect circularly polarized antenna AR is 0 dB. The following equation is used for determining AR in dB:

$$AR_{dB} = 20log_{10}\left(\frac{1+10^{-\frac{|U_{RHCP}-U_{LHCP}|}{20}}}{1-10^{-\frac{|U_{RHCP}-U_{LHCP}|}{20}}}\right) \quad (5)$$

where U_{RHCP} and U_{LHCP} are radiation intensities in dB for RHCP and LHCP signals. Axial ratio bandwidth describes a frequency range in which the antenna will be considered circularly polarized. For a classical unidirectional antenna, the axial ratio bandwidth will be the frequency range where AR is under 3 dB. Circularly polarized antenna can be realized either using dual

feeding or single feeding technique. However, this thesis will be focused on cpw-fed circularly polarized antennas with a single feeding technique.

Cpw-fed circularly polarized antennas:

Cpw-fed antenna allows easier fabrication, low cost, and smaller size while designing monopole antennas. Throughout the last decade, researchers have been proposing different types of structures for cpw-fed circularly polarized antennas. Zhai et al. [38] proposed a design with an asymmetric T-shaped feedline and an inverted L-shaped connected with the ground plane to realize an antenna with axial ratio bandwidth (ARBW) 62.6% working in 3.4 GHz – 6.5 GHz. A pentaband circularly polarized antenna is proposed using an I- shaped patch with a slot cut in the ground plane [39]. This shape shows excitation in 1.6 GHz, 2.45 GHz, and 3.45 GHz. A circular patch is printed to excite three more circularly polarized resonances. Chen et al. [40] proposed an antenna with a monopole radiator and an inverted L-strip on the ground plane to create asymmetric ground. Another antenna is proposed with a wide ratio bandwidth from 7.4 GHz to 10.2 GHz using two opposite L-shaped strips over the feedline and cutting the ground plane with different asymmetric rectangles [41]. Midya et al. [42] proposed an antenna by placing two orthogonal patches connected by optimized $\frac{\lambda}{4}$ microstrip line using the power divider technique with an axial ratio bandwidth of 520 MHz covering 4.9 GHz. Two circularly polarized bandwidths of 3.30 GHz – 3.78 GHz and 5.40 GHz – 5.86 GHz by placing two rectangular strips of different length on two opposite side over another rectangular patch connected with the feedline [43]. A ground stub is placed on the right side of the antenna to divide the fundamental modes into two different frequencies by influencing the larger magnetic current distribution. To generate RHCP and LHCP simultaneously, from 2.6 GHz – 5.9 GHz an antenna with two P-shaped radiators is proposed in [44]. However, none of this antenna are not on flexible substrate.

A cpw-fed flexible circularly polarized antenna is proposed on transparent polyethylene terephthalate polyester (PETP) film with an axial ratio bandwidth of 17.81% from 2.25 GHz – 2.69 GHz [45]. There are some other flexible antennas on different materials like PDMS [46] , [47], woolen felt [48], liquid crystal polymer (LCP) substrate [49], Panasonic R-F770 substrate [50] for different frequency ranges, which are challenging to fabricate.

CHAPTER TWO: INKJET PRINTED FLEXIBLE HIGH ISOLATION PATCH ANTENNA FOR 5.8 GHZ FULL DUPLEX APPLICATIONS

Introduction:

With the increase in the number of devices getting connected to the internet network, 5 GHz wifi band, which is more precisely from 5.725 GHz to 5.875 GHz, having a center frequency of 5.8 GHz, needs to be utilized more to prevent 2.4 GHz band from getting saturated. Moreover, implementing a full duplex antenna will double the spectral efficiency [1]. Full duplex transmission mode transmits and receives simultaneously in the same frequency band, making the number of devices used in the band twice and hence improving the spectral efficiency to double. However, full duplex mode needs around -100 dB isolation between transmit and receive signals. This -100 dB isolation can be achieved with combined efforts in antenna, analog circuits, and digital signal processing. Achieving isolation around -50 dB in antenna level helps to design other levels with less complexity and reduced cost.

Researchers have designed and characterized full duplex antennas on different materials targeting different frequency ranges. In [51], a full duplex antenna is proposed on FR4 epoxy substrate with ring hybrid feeding structure, and T-shaped defected ground structure (DGS) at 2.4 GHz. An antenna array is proposed in [17] with slotline based 180o hybrid structure to improve isolation to -50 dB at 4.75 GHz to 5.18 GHz. In [52], a broadband dual polarized meta surface based antenna is proposed to operate at 3.5 GHz for in band full duplex applications, where differential feeding scheme is applied to create high isolation. However, all of these antennas are on rigid materials meaning they are not suitable for flexible and wearable applications.

Recently, next generation devices are getting flexible in nature because of advantages like lightweight, cheapness, portability, and durability. Thus, the demand for flexible antennas is

increasing as it is one of the most essential elements for the flexible device. Materials like polyethylene terephthalate (PET), polyethersulphone (PES), polycarbonate (PC), polyimide (PI), polyethylene naphthalate (PEN), and polydimethylsiloxane (PDMS) are used as substrates for flexible antennas [53]. Textile based antennas are also getting much attention as it is a promising option or wearable antennas [54]–[56]. Inkjet printing [57], 3-D printing [58], screen printing [59], and chemical etching [60] are popular methods for antenna fabrication on polymer substrates, whereas stitching and embroidery [61] are used for textile antennas.

Flexible antennas working at 5.8 GHz are studied widely using different materials and printing processes. In [62], a microstrip-fed slot antenna is proposed for 5.3 GHz-6.3 GHz using PEDOT:PSS conductive polymer. A dual band CPW-fed antenna working in 2.44 GHz and 5.8 GHz bands using flexible Rogers Ultralam 3850 is proposed in [63]. Another dual band antenna is designed on denim material which works on 2.45 GHz and 5.8 GHz [64]. A wide band antenna working from 1 GHz to 8 GHz is proposed in [65] using kapton substrate. In another recent work [66], an ultra-wideband antenna operating from 5.2 GHz to 41 GHz is proposed, which is fabricated on liquid crystal polymer (LCP). However, none of these antennas have full duplex capacity. In [67], a textile antenna is proposed for 2.4 GHz full duplex wearable applications, where two additional strips are placed perpendicularly to the feed lines for improving bandwidth and isolation between ports. This work has reported -20 dB isolation, which is not very effective in full duplex systems due to low isolation. Similarly, in [68] and [69] dual-polarized antennas are proposed for on-/off-body wearable applications. Both designs demonstrate low isolation values between TX and RX ports, making them not suitable for full duplex systems. Another work [70] proposes a substrate integrated waveguide based (SIW) antenna operating at 4.8 GHz and 5.8 GHz

with an isolation level of -29.8 dB for wearable applications. However, this antenna also lacks the necessary level of isolation as well as a more complex fabrication process than other candidates.

In this section, an inkjet printed full duplex flexible antenna on PET substrate is proposed, which will work on 5.8 GHz and effectively can be used for flexible and wearable applications. The main contribution of this work is the proposal of a full duplex antenna on 5.8 GHz, as this will be one of the most used frequency bands in the near future. The proposed antenna shows measured high isolation of -68 dB in 5.8 GHz while maintaining a -10 dB bandwidth from 5.66 GHz to 5.95 GHz. Also, presenting it as a flexible device enhances its arena of applications. Simulation and experimental studies are carried out to show the effectiveness of the antenna for bending situations and human tissue loading. This antenna ushers the domain of designing flexible full duplex antenna. To the best of our knowledge, this design has the highest isolation achieved for flexible full duplex systems.

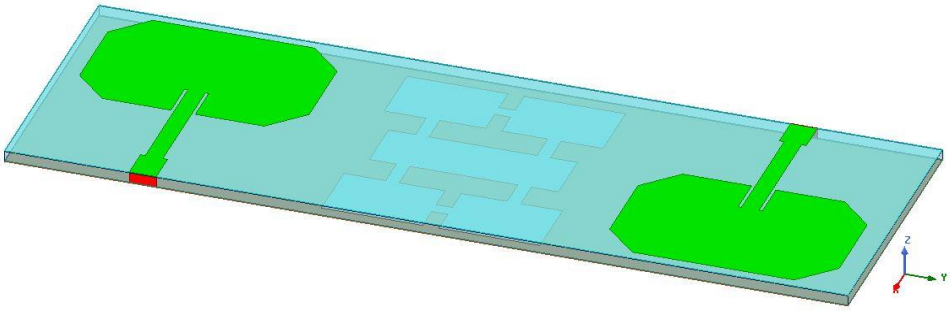

(a)

(b)

(c)

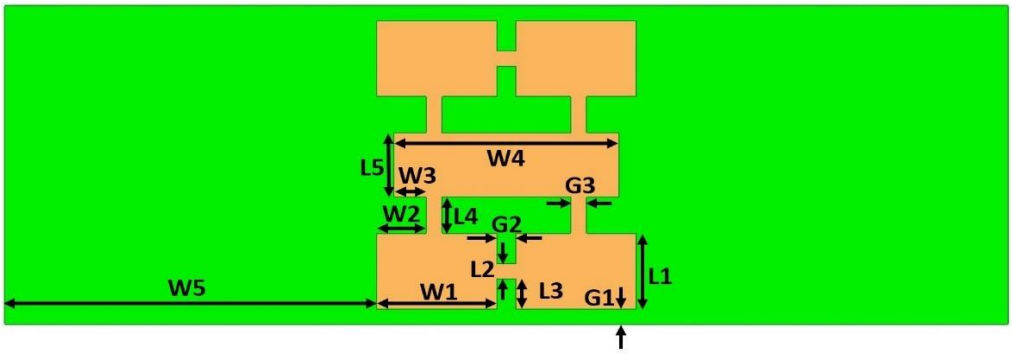

(d)

Figure 2.1: Proposed full duplex patch antenna. (a) Trimetric view, (b) Side view, (c) Top view with detailed parameter marking, (d) Bottom view with detailed parameter marking.

Antenna Design:

Design Configuration:

The proposed flexible antenna consists of three layers. Top and bottom layers are PET paper, and middle layer is foam. Each PET paper layer has a thickness of 0.135 mm, and the foam layer has a thickness of 1.6 mm. The relative permittivity of the PET paper is 3.2, and the loss tangent is 0.022. Commercially available low loss flexible foam from Cuming Microwave is used here, with a relative permittivity of 1.06 and a loss tangent of 0.0001. The length and width of the proposed antenna are 42 mm and 125 mm, respectively. In the top layer, two patches are printed with 84 mm distance between their feed lines, whereas one patch will be used for transmission and

another will be used for reception. The distance between these two patches is optimized for achieving more than -50 dB isolation throughout the band of operation. Microstrip line feeding technique with inset feeding is used here for greater impedance matching. DGS is printed in the bottom layer. DGS is used to obtain a better isolation level as it is placed between two patches. This antenna is designed and simulated using ANSYS HFSS. Optimized parameters for patch and DGS are given in Table 2.1. In Figure 2.1, the trimetric view, side view, top view, and bottom view with detailed parameter marking of the proposed antenna are shown. Figure 2.2 shows the simulated S-parameters of the proposed antenna. It can be depicted from the figure that the proposed antenna has -10 dB impedance bandwidth of 280 MHz (FBW = 4.8%) and a low mutual coupling reaching -85 dB at the center frequency.

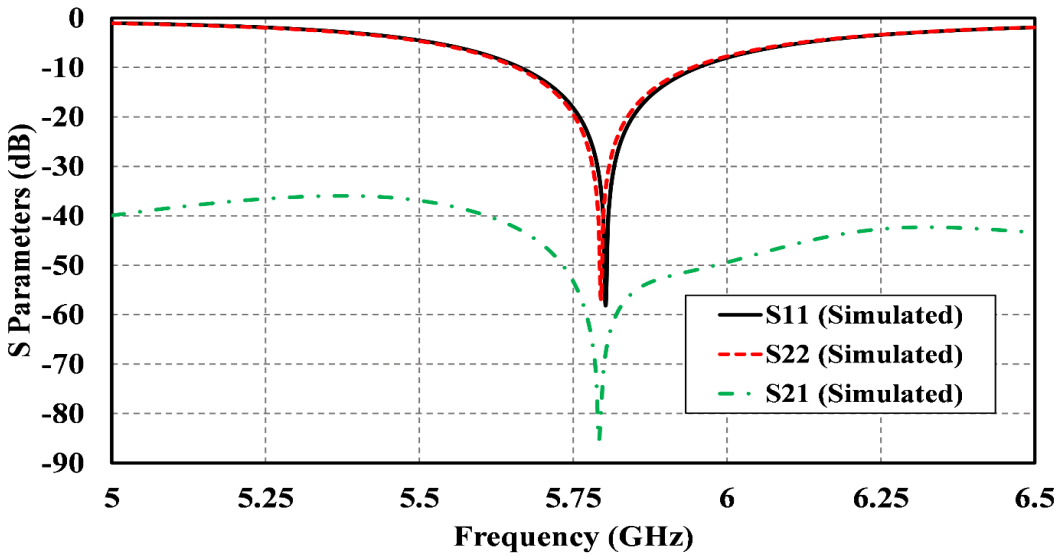

Figure 2.2: Simulated S parameters of the proposed antenna.

Table 2.1: Optimized parameters for the top and bottom layer designs of proposed antenna.

Parameter	Value, mm	Parameter	Value, mm
F1	18.5	L1	10
F2	4	L2	2
F3	10.2	L3	4
F4	15.2	L4	4.75
F5	34	L5	8.5
F6	2.6	W1	15
H1	12.93	W2	6.2
H2	5	W3	4
H3	22.5	W4	28
H4	12.5	W5	46.3
H5	5	G1	2
G2	2.4	G3	2

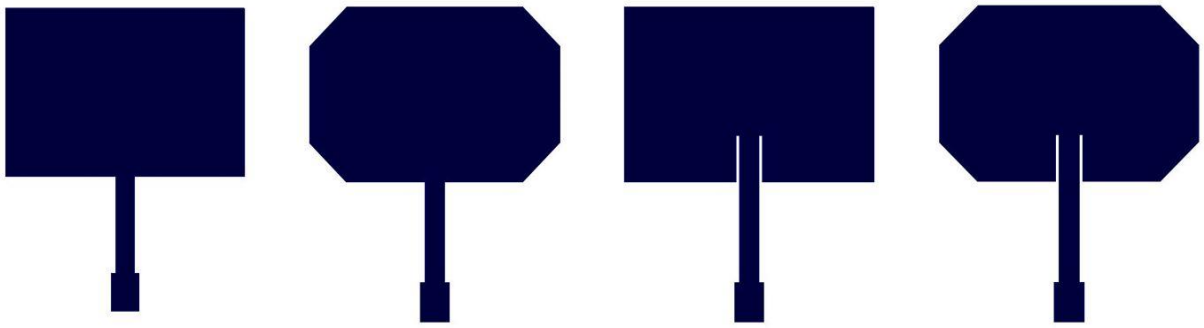

Figure 2.3: Evolution of the patch of the proposed antenna.

Patch design steps:

The evolution of the proposed antenna is shown in Figure 2.3. Firstly, patches of the top layer are designed only as simple rectangular patches. Simple rectangular patches have shown a bandwidth of 190 MHz from 5.26 GHz to 5.45 GHz. However, it does not have any bandwidth

under -50 dB for the S21 parameter. Secondly, corner cut in all four corners of both patches with the same size is introduced. After that, the antenna has resonance shifted to the right with a bandwidth of 130 MHz from 5.55 GHz to 5.68 GHz. Also, an isolation bandwidth of 150 MHz from 5.77 GHz to 5.92 GHz under -50 dB is obtained. However, this bandwidth under -50 dB is not workable because it is not in the range where the patch antenna works. After that, only inset feeding is introduced, which has increased impedance matching bandwidth to 220 MHz from 5.36 GHz to 5.58 GHz. In this case, a bandwidth of 200 MHz from 5.47 GHz to 5.67 GHz has been found under -50 dB for the S21 parameter. Moreover, this case shows a portion of bandwidth from 5.47 GHz to 5.58 GHz, which is workable. Finally, after combining the corner cut and inset feeding cases, a bandwidth of 280 MHz from 5.67 GHz to 5.95 GHz for the S11 parameter and a bandwidth of 250 MHz from 5.73 GHz to 5.98 GHz for the S21 parameter is achieved. Design steps are compared for the S11 and S21 parameters, which are given in Figure 2.4 and Figure 2.5, respectively.

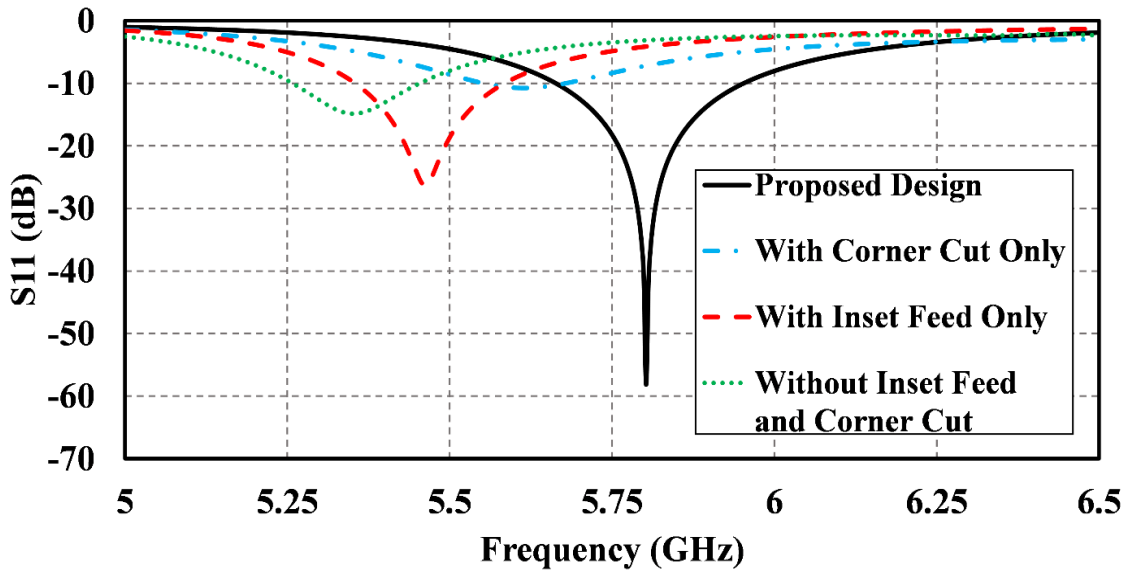

Figure 2.4: Simulated S11 parameters for different patch design steps.

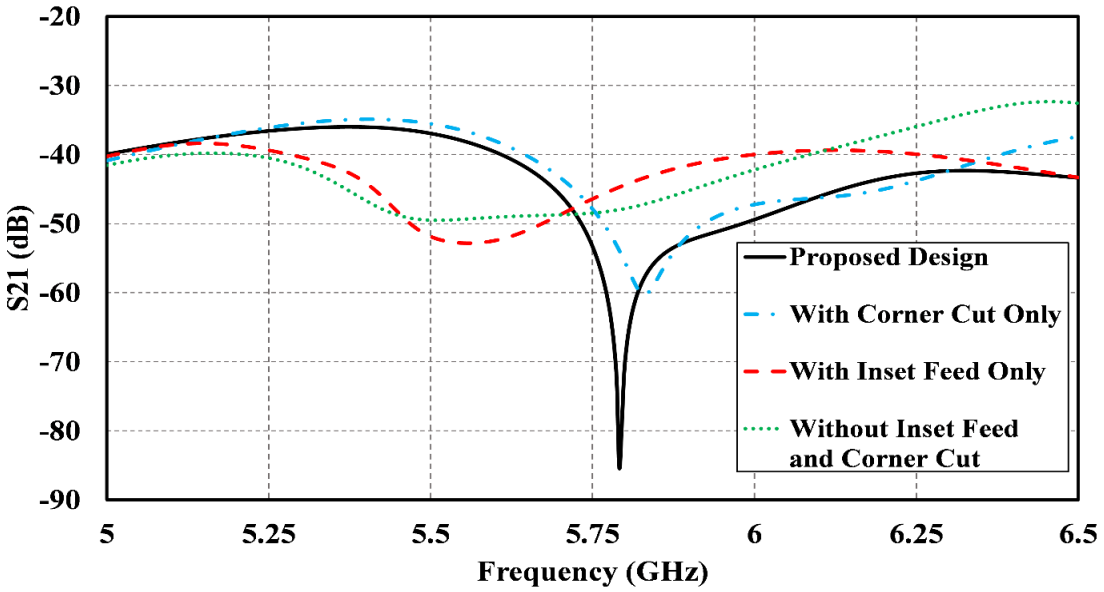

Figure 2.5: Simulated S21 parameters for different patch design steps.

Impact of DGS:

DGS are particularly useful for cross polarization suppression [71], higher order harmonics reduction [72], bandwidth enhancement [73], isolation improvement [74], and for improving radiation properties [75]. Different shapes like dumbbell, open arrowhead, spiral head, "H" shape, "U" shape, vertically periodic, and horizontally periodic are already proposed for these purposes for microstrip patch antenna as it also offers integration without any spacing or circuit modeling complexity [76]. DGS causes disturbance in surface current distribution that ultimately results in increased effective inductance and capacitance.

A closed rectangular loop with rectangles in corners is designed in the proposed DGS. Another rectangle is placed in the middle, which is also connected to the loop. The structure is placed in between two patches. A difference is recorded in the S21 parameter after introducing the DGS, which is shown in Figure 2.6. Without DGS, S21 has a bandwidth of 80 MHz from 5.79

GHz to 5.87 GHz, whereas the bandwidth is 250 MHz with DGS. Also, the minimum S21 is -50.65 dB and -85 dB without DGS and with DGS, respectively. In Figure 2.7, it is shown that surface currents are being accumulated around DGS, which reduces the mutual coupling between TX and RX ports. It proves the impact of DGS in isolation improvement. This simulation is done at 5.8 GHz.

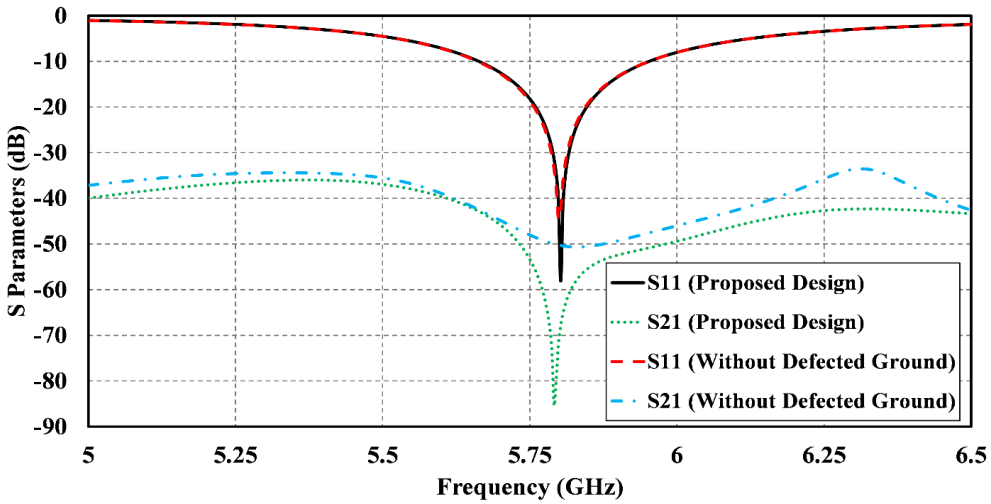

Figure 2.6: Simulated S parameters comparison of the antenna with and without DGS.

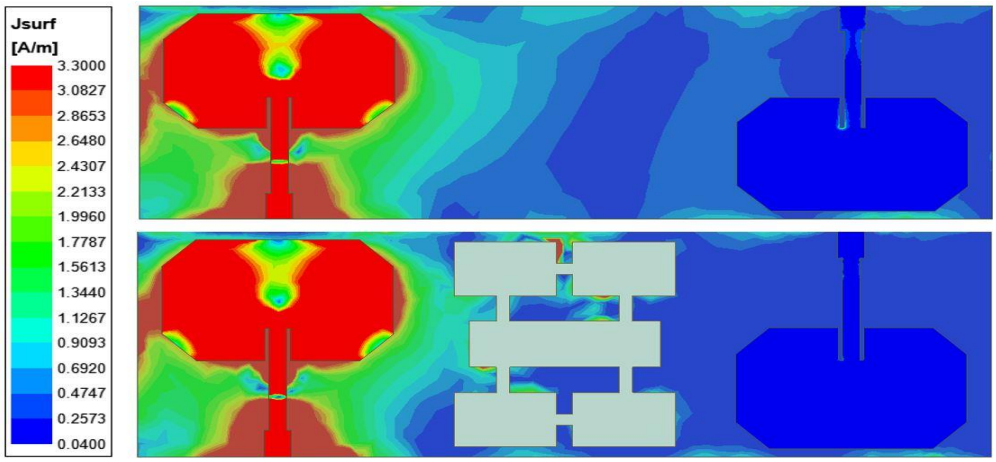

Figure 2.7: Simulated surface current density comparison of the antenna without and with DGS at 5.8 GHz.

Impact of inserting foam in between:

Another important feature of the proposed design is of using foam between the top and bottom PET paper layer. A low loss, flexible foam is used for this purpose. The reason for using foam in between is to provide better structural stability and bandwidth improvement. The foam layer and PET paper layers are attached using glue in between. In Figure 2.8, simulated S parameters are compared by placing foam and air between PET paper layers. S11 parameters have shifted when the foam is used instead of air. For air, bandwidth is around 290 MHz from 5.78 GHz to 6.07 GHz, whereas for foam bandwidth is around 280 MHz from 5.67 GHz to 5.95 GHz. Also, S21 is not under 50 dB for any frequency range when air is in between PET paper layers, whereas S21 has a bandwidth of 250 MHz from 5.73 GHz to 5.98 GHz when the foam is used. Also, the antenna is examined without any gap in between by placing two PET paper layers together. As expected, it shifts the resonant frequency at 5.34 GHz with a smaller bandwidth of 95 MHz. The resonant frequency is reduced as effective permittivity is increased due to the removal of the foam layer. Therefore, the foam has important contributions to obtaining desired antenna parameters.

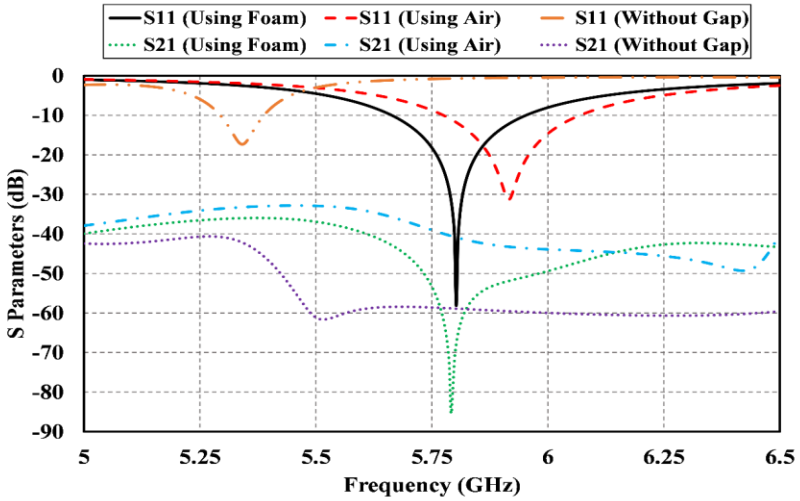

Figure 2.8: Simulated S parameters comparison for foam and air in between top and bottom PET paper layers.

Table 2.2: Properties of skin, fat and muscle layer at 5.8 GHz [77].

Tissue	Permittivity	Conductivity, S/m	Density, kg/m^3	Loss tangent
Skin	35.114	3.717	1090	0.418
Fat	4.9549	0.29313	1150	0.186
Muscle	48.485	4.9615	1050	0.342

Human phantom loading:

As this antenna has the option to be used as a wearable one, antenna performance needs to be investigated when it is loaded with human tissue. A tissue mimicking phantom model is created by placing layers of muscle, fat, and skin on top of each other, respectively, as shown in Figure 2.9 (a). The electrical properties of these layers can be found using Debye equation which can be expressed as [78],

$$\varepsilon_\tau = \varepsilon_\infty + \frac{\varepsilon_s - \varepsilon_\infty}{1+j\omega\tau} - j\frac{\sigma_s}{\omega\varepsilon_o}, \quad (1)$$

Here, "ϵ_τ" refers to complex permittivity, "ϵ_∞" refers to optical permittivity, "ϵ_s" refers to static permittivity, "ω" is angular frequency, "τ" is relaxation time, "σ_s" is conductivity and "ϵ_o" is free space permittivity. In Table 2.2, the electrical properties of the layer, which are found in (1) are listed for 5.8 GHz frequency. The permittivity of the skin and muscle layer is high as they have more water content present and has a significant influence on the electric field.

To simulate the effect of human phantom loading, the proposed antenna is placed over a human phantom structure consisting of skin, fat and muscle layers. The size of the phantom structure is 70 x 150 mm^2. The skin, fat, and muscle layer height is 2 mm, 5 mm, and 20 mm, respectively. In Figure 2.10 (a), the S11 parameter for different gap distances between the antenna

and the phantom is analyzed. A small amount of shifting in resonant frequency is observed from 5.77 GHz to 5.82 GHz, while the gap between the antenna and phantom is increased from 0 mm to 2 mm. Similarly, in Figure 2.10 (b), the S21 parameter of the antenna is analyzed. For 0 mm and 1 mm gap distance, isolation was below -50 dB in 5.8 GHz, while it went down to -47 dB for 2 mm gap distance due to the distraction of electric field distribution by the electrical properties of the phantom layer.

To analyze the impact of clothing on antenna performance, a fabric layer is also added over the skin layer, as seen in Figure 2.9 (b). The antenna is simulated with two different fabrics (fleece and leather). The permittivity of the fleece and leather layer is 1.17 and 2.95, along with loss tangents of 0.0035 and 0.006, respectively [79]. The fleece and leather layers have a thickness of 0.05 mm and 0.5 mm, which are the conventional thickness for these fabrics. Figure 2.10 (c) – 2.10 (f) shows S parameters when the antenna is simulated over the phantom model with fabric layers. As seen, S11 and S21 show similar patterns even after applying these two different kinds of fabrics. Therefore, it can be remarked that S parameters are not affected significantly due to human phantom loading even after placing over textile materials.

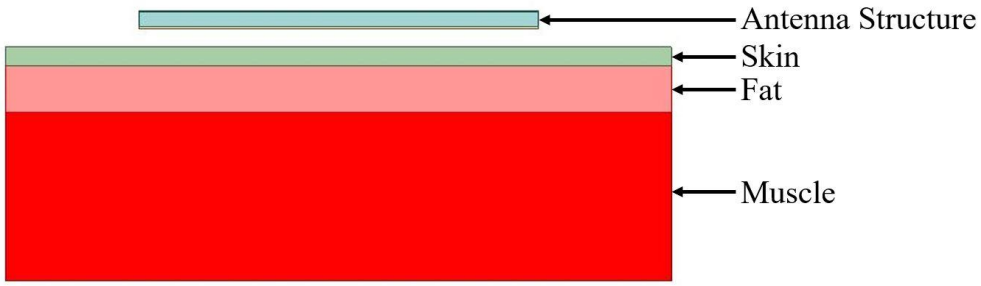

(a)

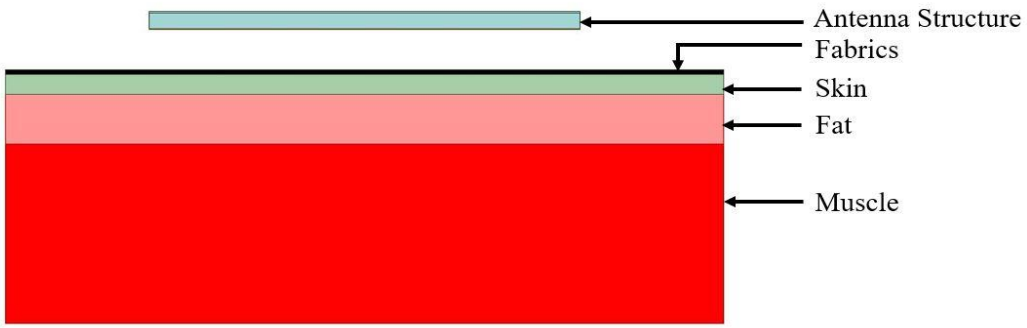

(b)

Figure 2.9: Side view of the antenna over the phantom model (a) without skin, (b) with skin.

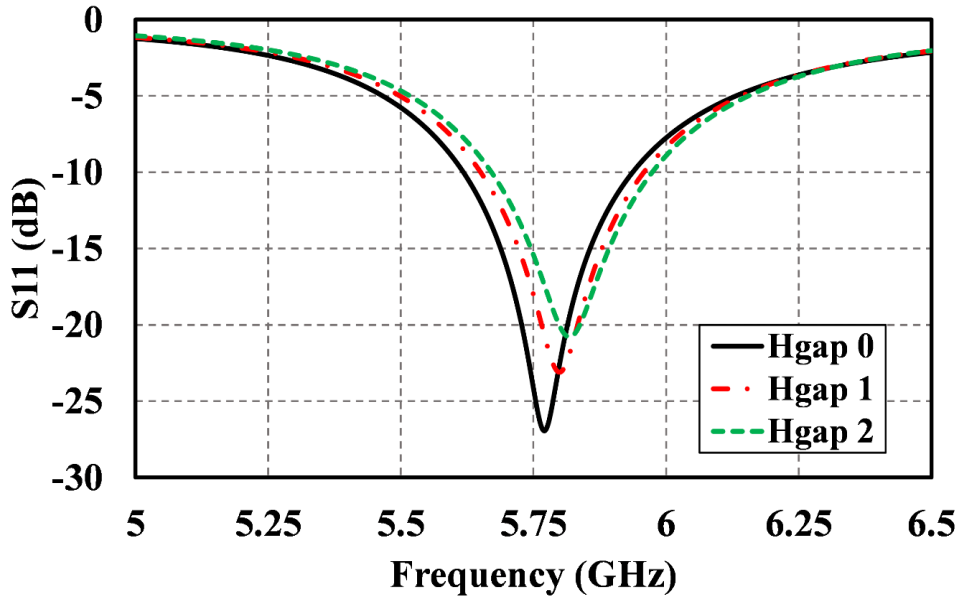

(a)

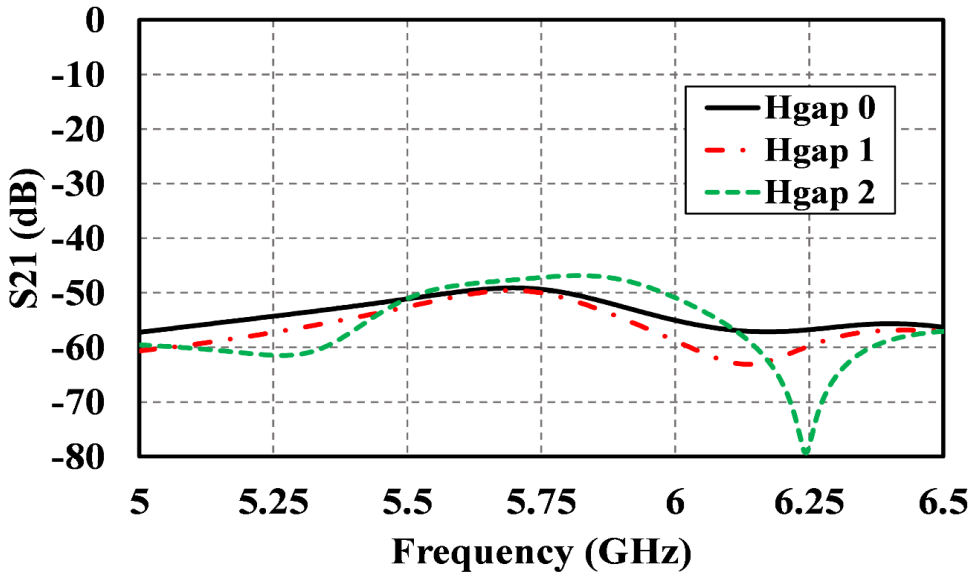
0
-10
-20
-30
-40
-50
-60
-70
-80
S21 (dB)
5
5.25
5.5
5.75
6
6.25
6.5
Frequency (GHz)
Hgap 0
Hgap 1
Hgap 2

(b)

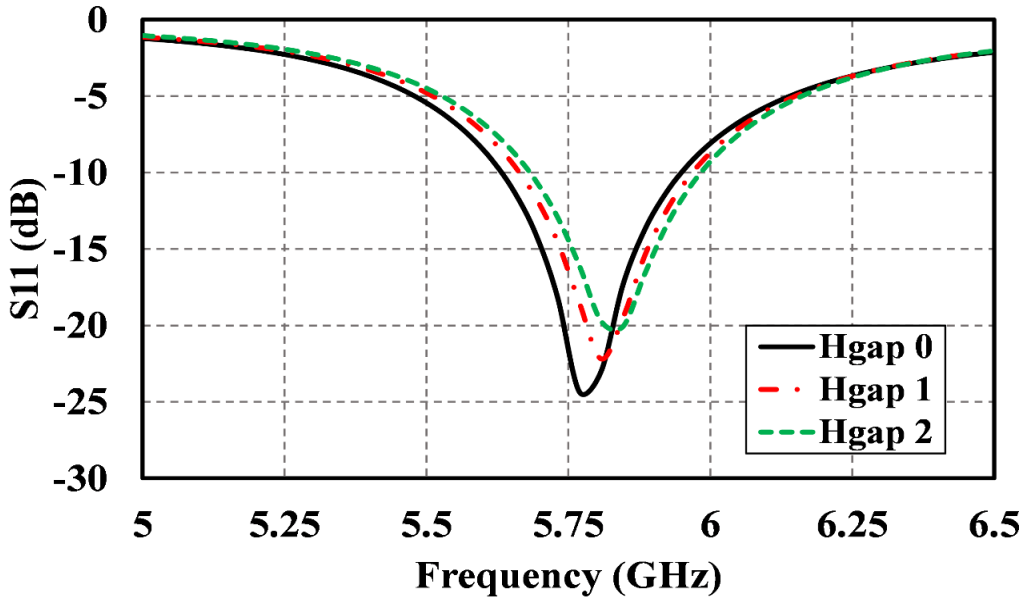
0
-5
-10
-15
-20
-25
-30
S11 (dB)
5
5.25
5.5
5.75
6
6.25
6.5
Frequency (GHz)
Hgap 0
Hgap 1
Hgap 2

(c)

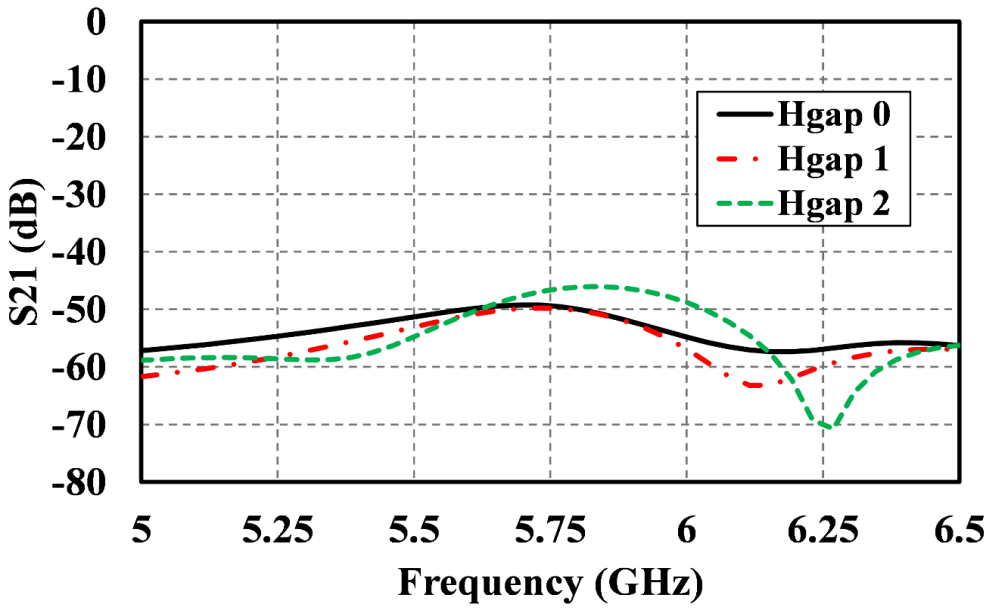
0
-10
-20
-30
-40
-50
-60
-70
-80
S21 (dB)
5
5.25
5.5
5.75
6
6.25
6.5
Frequency (GHz)
Hgap 0
Hgap 1
Hgap 2

(d)

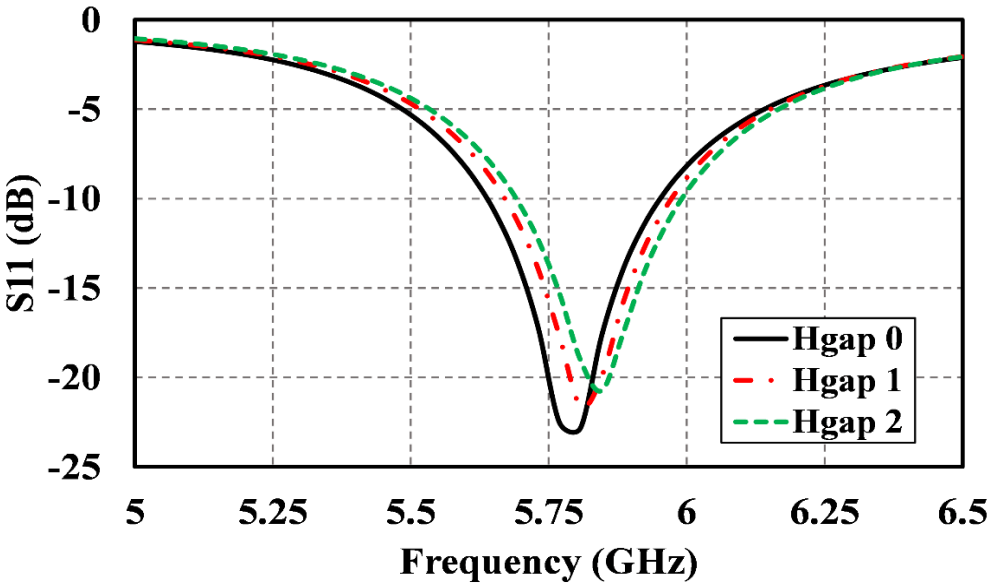
0
-5
-10
-15
-20
-25
S11 (dB)
5
5.25
5.5
5.75
6
6.25
6.5
Frequency (GHz)
Hgap 0
Hgap 1
Hgap 2

(e)

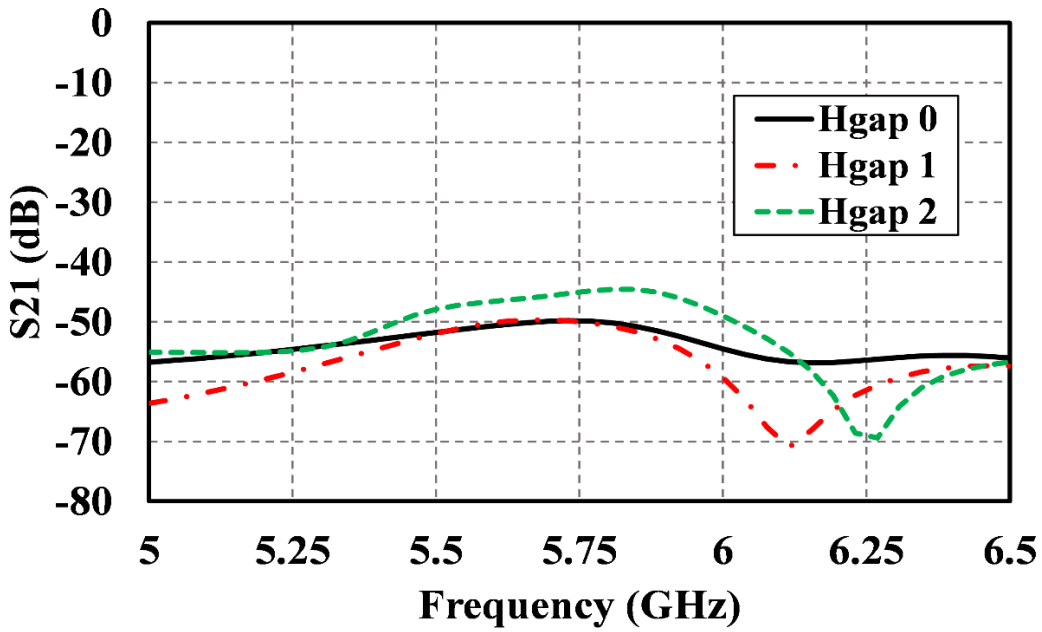

(f)

Figure 2.10: Simulated (a) S11 parameter, (b) S21 parameter directly over skin, (c) S11 parameter, (d) S21 parameter over fleece fabrics, (e) S11 parameter, (f) S21 parameter over leather fabrics comparison for different positions of the antenna over the phantom model.

Specific absorption rate (SAR) analysis:

As the proposed antenna can be used for wearable applications, radiated electromagnetic energy must be kept under the limit of health hazards. SAR values are used as the parameter to ensure the safe usage of wearable antennas. The value of SAR can be calculated from the equation below:

$$SAR = \frac{\sigma |E|^2}{\rho} \quad (2)$$

where σ is the conductivity of the tissue in S/m, and ρ is the mass density of the tissue in kg/m^3.

According to IEEE C95.1-2005 standard, SAR value should be under 1.6 W/kg over 1g tissue. To evaluate SAR, an input power of 100 mW is applied to both ports. The antenna is set on top of the phantom described in the previous section.

In Figure 2.11 (a), the distribution of the SAR field over the antenna is demonstrated. The electric field is mostly accumulated in the region of the ports and patches as expected. In Figure 2.11 (b), the average SAR is shown varying the gap between the antenna and the human phantom. SAR value has touched the 1.6 W/kg constraints when the gap is 0 mm. However, the value sharply decreases when the gap is introduced. At 1 mm and 2 mm gap, the average value of SAR is 0.9678 W/kg and 0.8549 W/kg, respectively. The value keeps itself around 0.8 W/kg if the gap distance continues to increase, which fulfills the condition of safe wearable use of the antenna. Moreover, as previously stated, SAR value is determined over fleece and leather fabrics. At 0 mm gap, the SAR value is slightly over our constraint (1.7715 W/kg) for fleece. However, it drastically reduces to 1.0231 W/kg after increasing the gap to 1 mm and reduces further as the gap increases. For leather, the SAR value is well below the constraint for any gap value (1.4898 W/kg for 0 mm). Therefore, the antenna is also safe for usage over clothing.

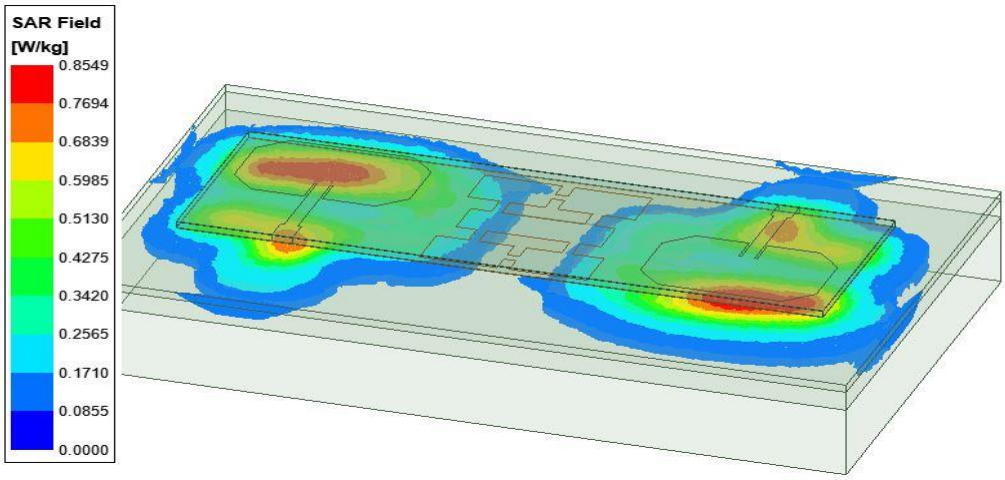

(a)

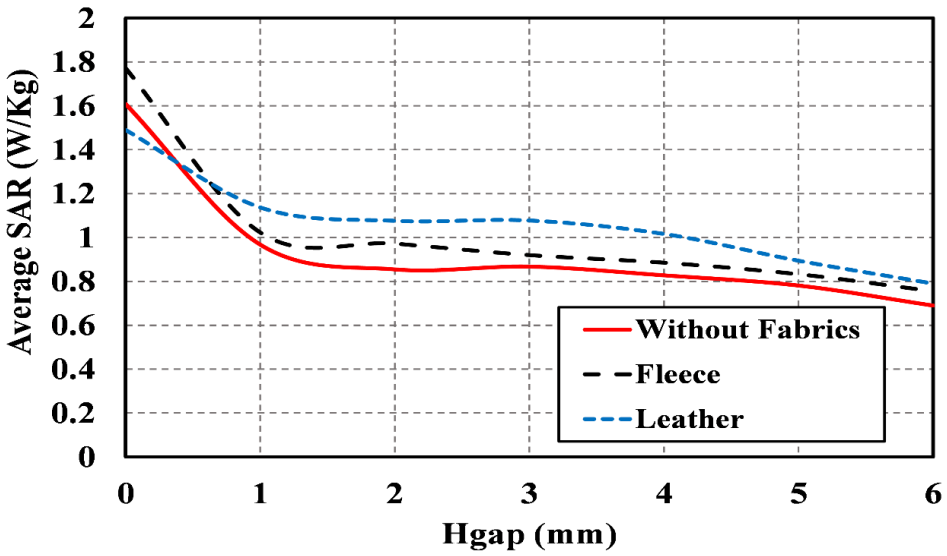

(b)

Figure 2.11: (a) Simulated 1 g averaged SAR in the tissue with a gap of 2 mm between antenna and phantom, (b) Simulated average SAR with respect to the the gap of antenna and phantom (Hgap).

Radiation efficiency and gain analysis:

Figure 2.12 shows the peak gain and radiation efficiency of the antenna with and without contact with the human phantom. The peak gain of the antenna at 5.8 GHz is 9.22 dB while maintaining over 9 dB in the whole 5.73 GHz to 5.95 GHz. When the antenna is placed 2 mm over the human phantom, the peak gain is increased to around 11 dB. This increase in gain happens because of the reflection of radiated waves from the human phantom as it is placed in close proximity (at around 0.04λ) [79]. Radiation efficiency is over 90% over the whole 5 GHz to 6.5 GHz bandwidth with 92.2% at 5.8 GHz. However, it decreases to 82% at 5.8 GHz while the antenna is put over the phantom due to the highly lossy characteristics of the phantom.

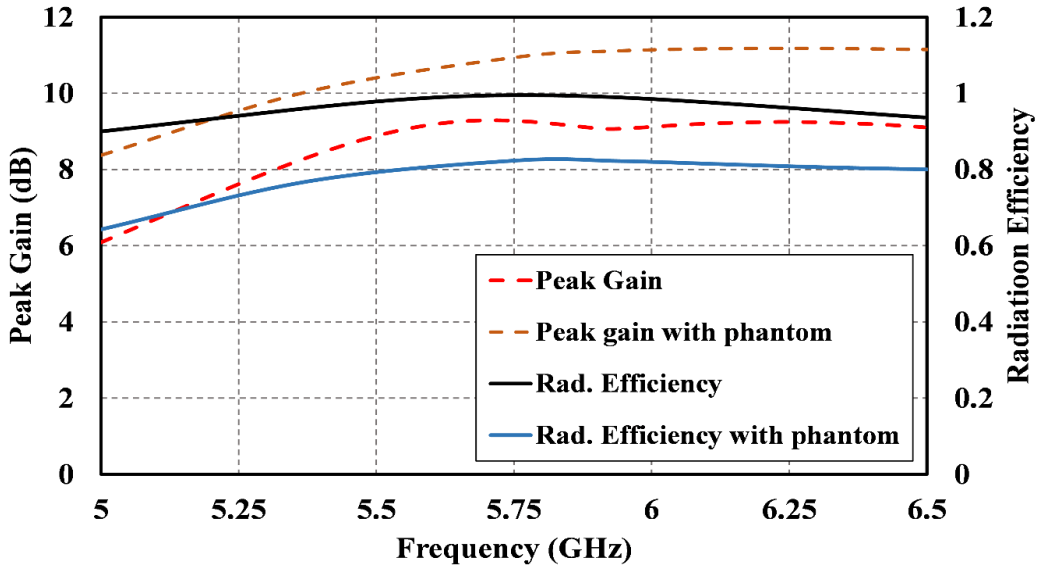

Figure 2.12: Peak gain and radiation efficiency of the proposed antenna.

Results and discussion:

This antenna is fabricated using a Fujifilm Dimatrix 2831 Inkjet printer (DMP), which uses a 10 pL cartridge having 16 nozzles with each having diameter of 21 µm. These nozzles are operated based on the deformation of a piezoelectric material which is placed as the wall of the ink channel. Silver nanoparticle ink from Novacentrix is used. The printed antenna is sintered on the hotplate using 120°C temperature to generate constant conductivity over the whole printed area. After printing the top and bottom layer, "3M Super 77 Multipurpose Adhesive" is used to attach them to the foam layer. SMA ports are connected using the conductive soldering gel, and hot air is blown over the connecting region to ensure connectivity. The fabricated antenna is tested using Keysight Fieldfox N9952A microwave analyzer. Figure 2.13 shows some steps of fabrication and characterization of the proposed antenna.

Figure 2.14 shows the comparison of the S11, S21, and S22 parameters of the proposed antenna. S11 and S22 parameters work under -10 dB in the proposed bandwidth for the fabricated

antenna. Measurement shows a slightly wider bandwidth than the simulation. The differences between the experiment and simulation are attributed to the imperfection of the fabrication due to the uneven ink layer distribution by the inkjet printer.

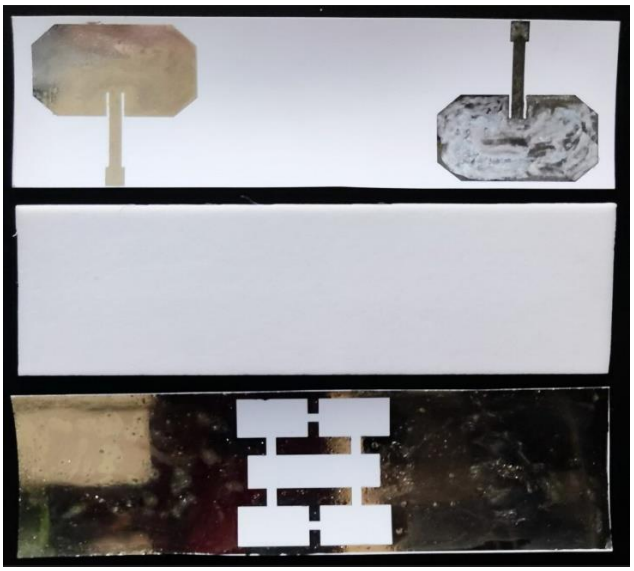

(a)

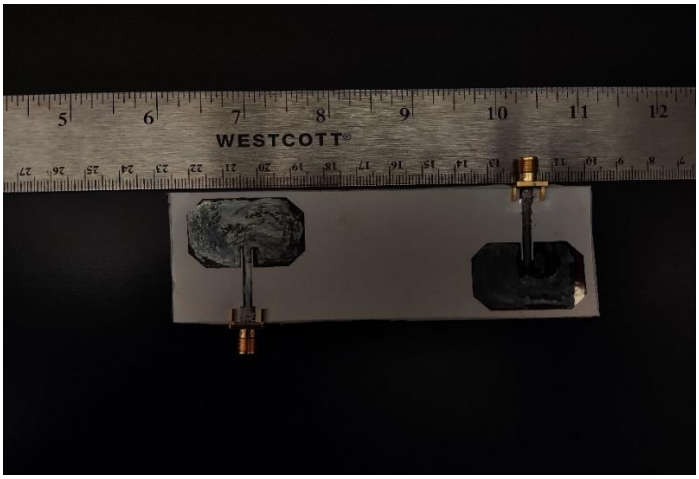

(b)

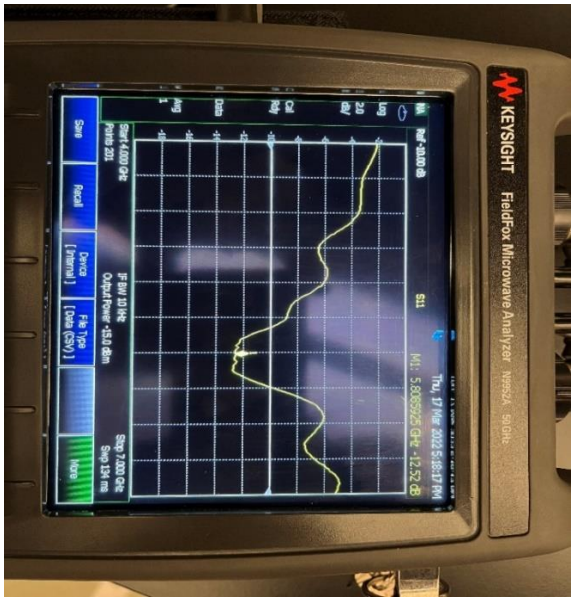

(c)

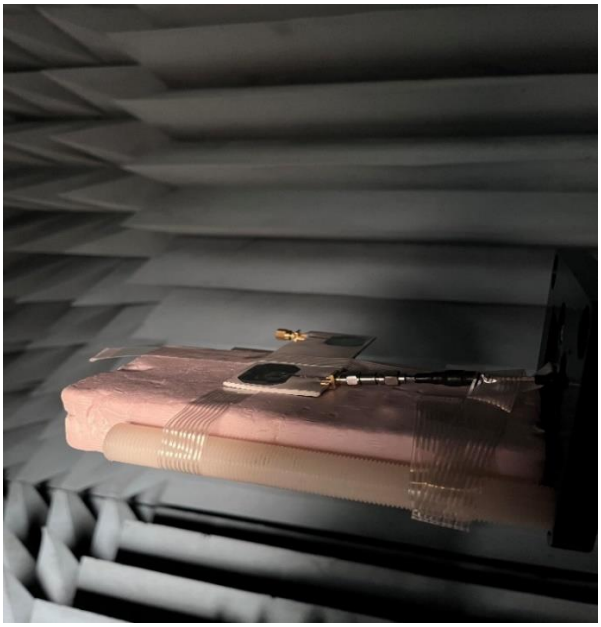

(d)

Figure 2.13: Images of fabricated antenna. (a) Top layer, foam and bottom layer, (b) Glued and soldered final version, (c) Testing with network analyzer, (d) Antenna in the anechoic chamber.

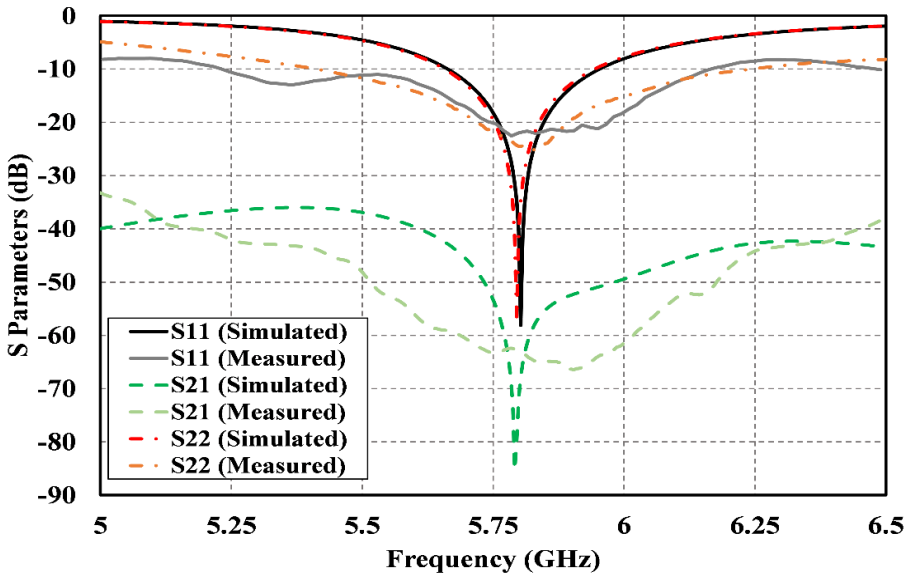

Figure 2.14: Measured and simulated S parameters of the proposed antenna.

Figure 2.15 shows the placement of antenna over the curved surface for bending tests, which are performed in two directions. The bending radius for this experiment is 5 cm. For diagonal bending case, antenna is placed exactly at 45°. Measured S-parameters of the bent antenna are given in Figure 2.16. S11 is under -10 dB for both parallel and diagonal bending from 5.6 GHz to 6.04 GHz, which is similar to the unbent case. However, resonant frequency shifts to 5.9 GHz, which is due to a change in effective permittivity as it was placed over a paper towel roll during measurement. The S21 parameter is under -50 dB for the whole bandwidth. Hence, the antenna maintains a robust performance in desired bandwidth.

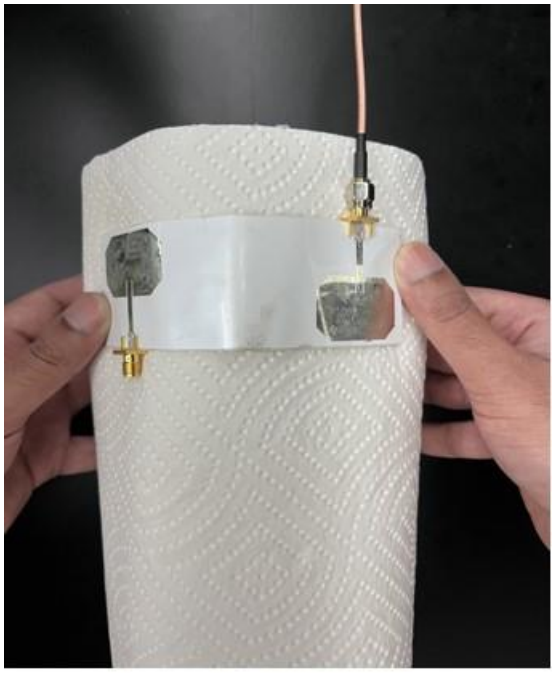

(a)

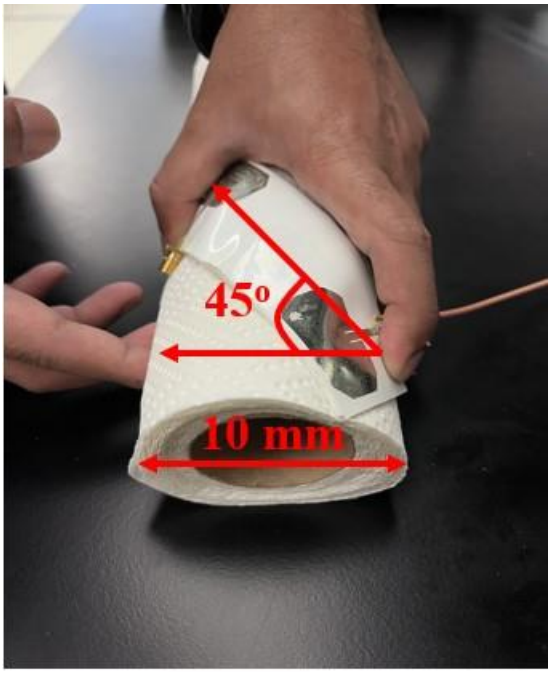

(b)

Figure 2.15: Antenna is bent (a) parallelly to the patch, (b) diagonally to the patch.

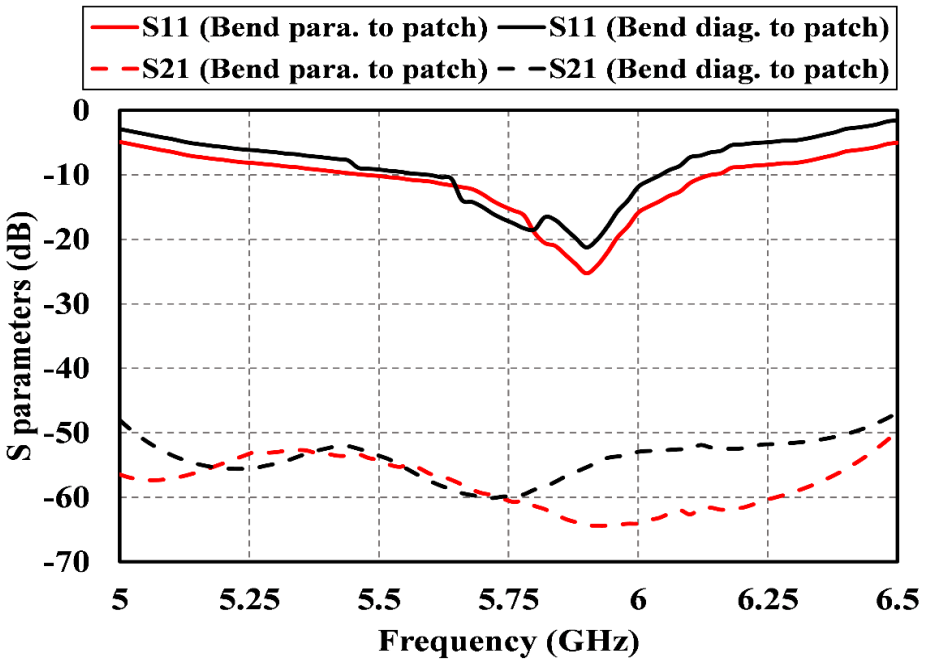

Figure 2.16: Measured effect of bending on S parameters of the proposed antenna.

To assess and characterize antenna performance for on body applications, the antenna is placed over different body parts like the belly and arm (see Figure 2.17). As shown in Figure 2.18, there is a slight shift in the resonant frequency (around 5.65 GHz) compared to free space measurement. However, it maintains S11 below -10 dB at 5.8 GHz while maintaining -50 dB isolation simultaneously. These measurements demonstrate that the proposed antenna is robust in human loading conditions.

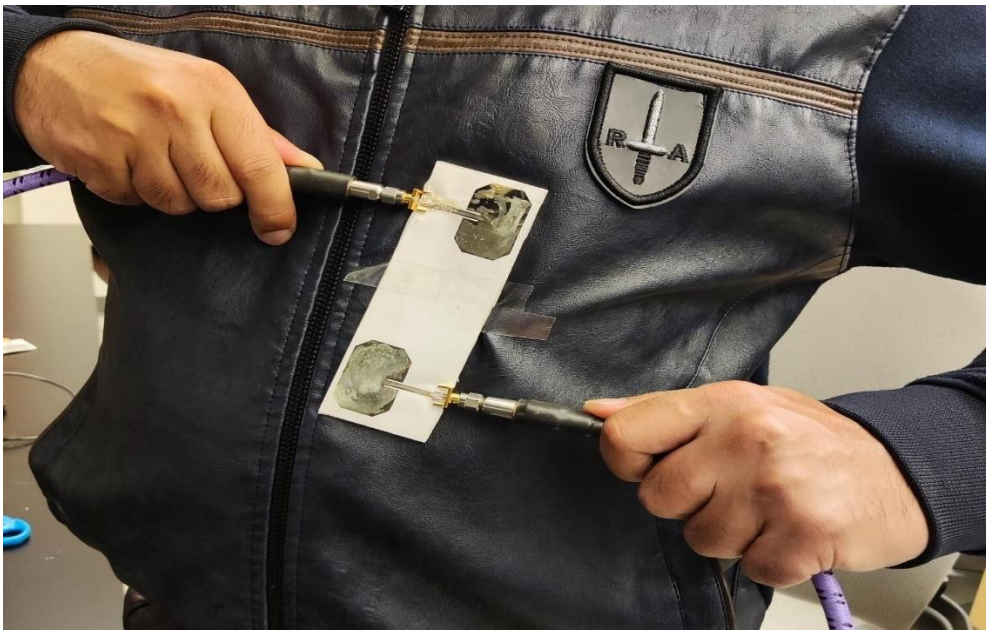

(a)

(b)

Figure 2.17: Proposed antenna tested on different parts of the body (a) Belly, (b) Arm.

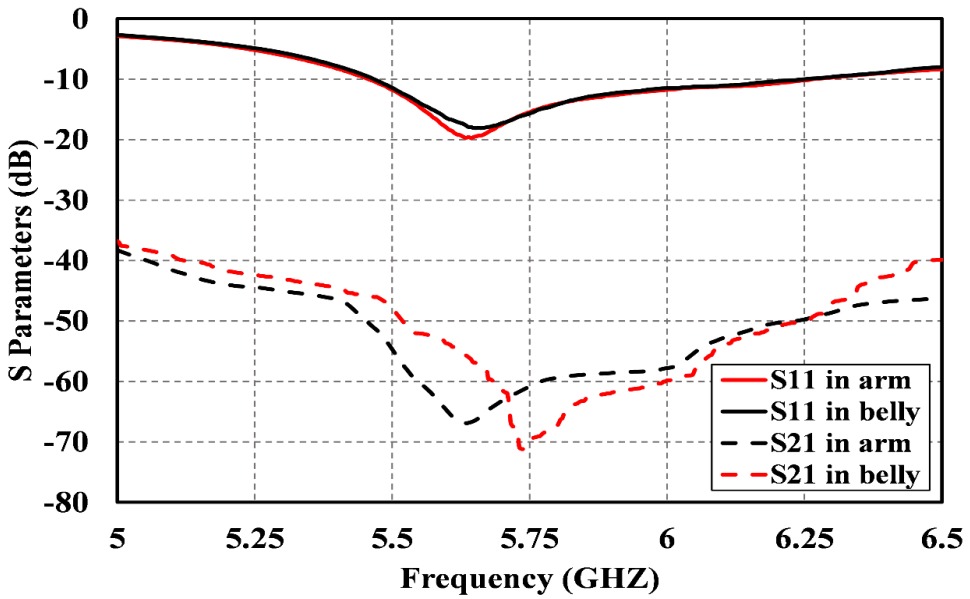

Figure 2.18: Measured S parameters for on body characterization.

Table 2.3: Comparison of proposed antenna with previously proposed full duplex works.

Reference	Resonant frequency, GHz	Fractional bandwidth	Isolation, dB	Peak gain, dB	Flexibility	Dimensions
[51]	2.4	5%	≤-35	4	No	0.68λ x 0.496λ x 0.012 λ
[17]	4.75 - 5.18	8.66%	≤-50	11	No	3.04λ x 0.99λ x 0.075λ
[67]	2.4	4.8%	≤-20	7.5	Yes	-
[68]	2.4	4.2%	≤-15	8.4/2.5	Yes	-
[69]	5.8	6.9%	≤-20	4/6	Yes	4.64λ x 0.77λ x 0.046λ
[70]	4.9, 5.8	4.08%, 4.65%	≤-29.8	5.75, 6.49	No	λ x 1.22λ x .33λ
[36]	3.3	2.4%	≤-36	4.3	No	0.56λ x 0.56λ x 0.0017λ
[80]	2.4	3.67%	≤-15	4.2	Yes	3.14λ x 0.23λ x 0.026λ
Proposed work	**5.8**	**4.8%**	**≤-50**	**9.22**	**Yes**	**2.41λ x 0.81λ x 0.036λ**

In Figure 2.19, normalized co-polarized and cross-polarized E and H plane pattern for the simulated and measured case at 5.8 GHz is shown. The antenna is measured by exciting one port and terminating the other port with a 50 Ω load. It is shown that the measured and simulated patterns match very well for both cases, with minor discrepancies due to measurement tolerance. The antenna shows unidirectional characteristics in the boresight with a very low amount of radiation in the back lobe. Co and cross-polarized planes maintain a difference of 20 dB in the boresight direction for both planes. In Table 2.3, the proposed antenna is compared with previously reported full duplex antennas from the literature. As seen, the current design differs from recent full duplex antennas by achieving the largest isolation level in addition to being flexible for wearable applications. Also, the design has comparable bandwidth and peak gain with the literature. Please note that the majority of antennas introduced are on rigid substrates (i.e. [17], [36], [51], [70]), and are not suitable for conformal full duplex applications. Compared to recent flexible full duplex implementations ([67]–[69], [80]), the proposed antenna has much higher isolation (<-50 dB) in the band of interest. From Table 2.3, it is seen that the highest isolation measured so far for flexible antennas is -20 dB. These designs will need to cancel an additional -30 dB for use in a full duplex system. The extra burden on analog and digital cancellation circuits will increase the cost and complexity of the overall system. While [69], which has the same center frequency, reports a higher bandwidth, the proposed design has higher measured isolation between transmit and receive ports and smaller size. Furthermore, although [51] and [36] have smaller sizes, both designs do not have flexibility and demonstrate lower measured isolation levels. Similarly, [52] has a high fractional bandwidth at the expense of a larger size.

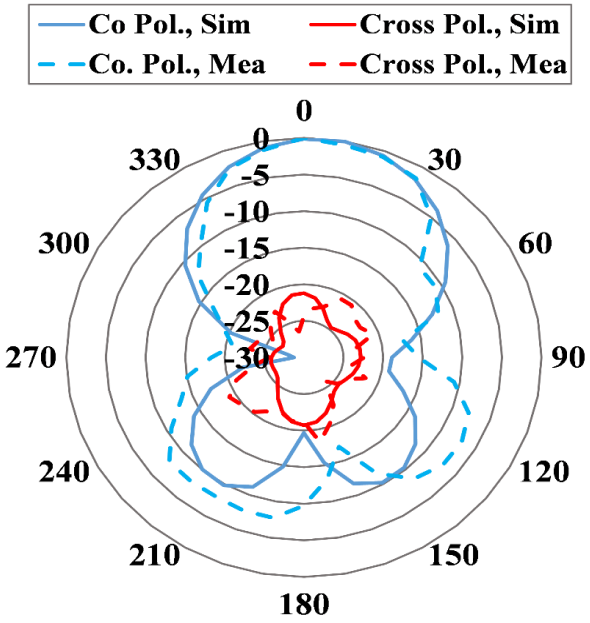

(a)

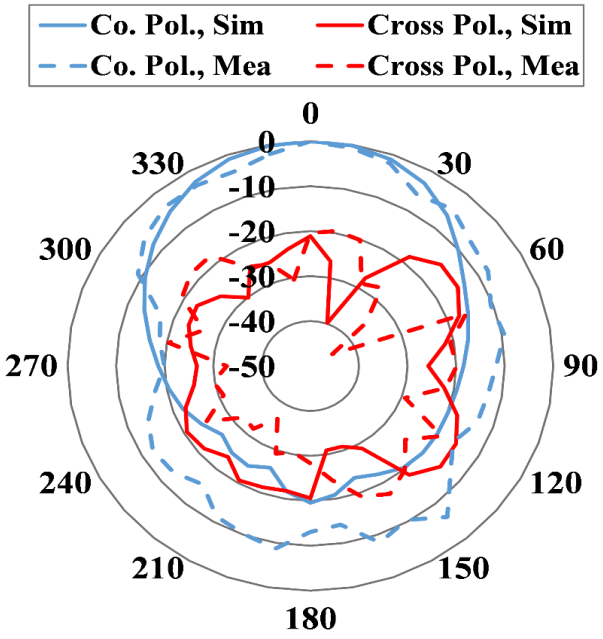

(b)

Figure 2.19: Normalized simulated and measured radiation pattern of (a) E plane and (b) H plane at 5.8 GHz.

CHAPTER THREE: CPW-FED COMPACT CIRCULARLY POLARIZED FLEXIBLE ANTENNA FOR C BAND APPLICATIONS

Introduction:

Demand for flexible electronics is projected to be around 50 billion US dollar globally by 2027 according to a recent market research. Antenna being an important part of modern devices, is extensively researched to make it compatible for flexible devices [53], [57]. However, most of these designs are linearly polarized antenna which are least preferred for non-stationary applications. Circularly polarized (CP) antennas provide advantages like low polarization mismatch loss, reduced multipath interference or fading which limits “Faraday rotation” effect, and less constraints for orientation in devices which result in enhancement of efficiency and reliability of moving wireless communication devices. Mainly dual feeding (uses complex structures like wilkinson power divider, ring hybrid coupler, and T junction power splitter etc.), and single feeding (CPW-feeding) are used for realizing CP antennas. Though dual feeding techniques offer wide bandwidth, CPW-feeding techniques are simple, compact, and easier to fabricate. In [81], an inkjet-printed circularly polarized antenna array is proposed for 7.4 GHz - 8.4 GHz. This design is bigger in size and is not in our band of interest. In [82], a CP antenna is proposed using Rogers Ultralam 3850 substrate for 5.2 GHz, which has very narrow bandwidth to work with. In [50], a flexible CP antenna is proposed for 5.73 GHz - 5.95 GHz using Panasonic R-F 770 substrate and foam where CP radiation is realized by putting two pairs of shorting pins on a regular rectangular patch antenna. This structure is complex to fabricate and have a relatively narrow bandwidth. In this section, a CP antenna is proposed for 4.07 GHz - 4.52 GHz axial ratio bandwidth (ARBW) by using inkjet printing on a PET paper layer. The antenna is 31 mm x 38

mm x 0.135 mm in size making it a very compact structure. Along with that, CPW-feeding is used to make the structure very simple to fabricate.

Antenna design:

The top layer of the proposed antenna is shown in Figure 3.1. Patch of the antenna is modified “S” shape with CPW feeding. This design is printed over a PET paper which has a thickness of 0.135 mm, loss tangent of 0.022 and permittivity of 3.2. The length of the antenna is 31 mm and width is 38 mm. Antenna design is upgraded step by step which is shown in Figure 3.2. Firstly, a slot with a width of 0.5mm is introduced in the ground plane. The location of the slot is left side of the feed line. The gap between the ground plane and the feed line is 0.57 mm in both sides. Three slots are inserted in the patch of the antenna which are marked in Figure 3.1. All these slots have same width of 0.2 mm while slot “A”, “B”, and “C” has length of 3.9 mm, 6.9 mm, and 4 mm respectively. Inset feeding is used in this antenna with a distance of 3 mm from the end. Other parameters are optimized using ANSYS HFSS and shown in Figure 3.1.

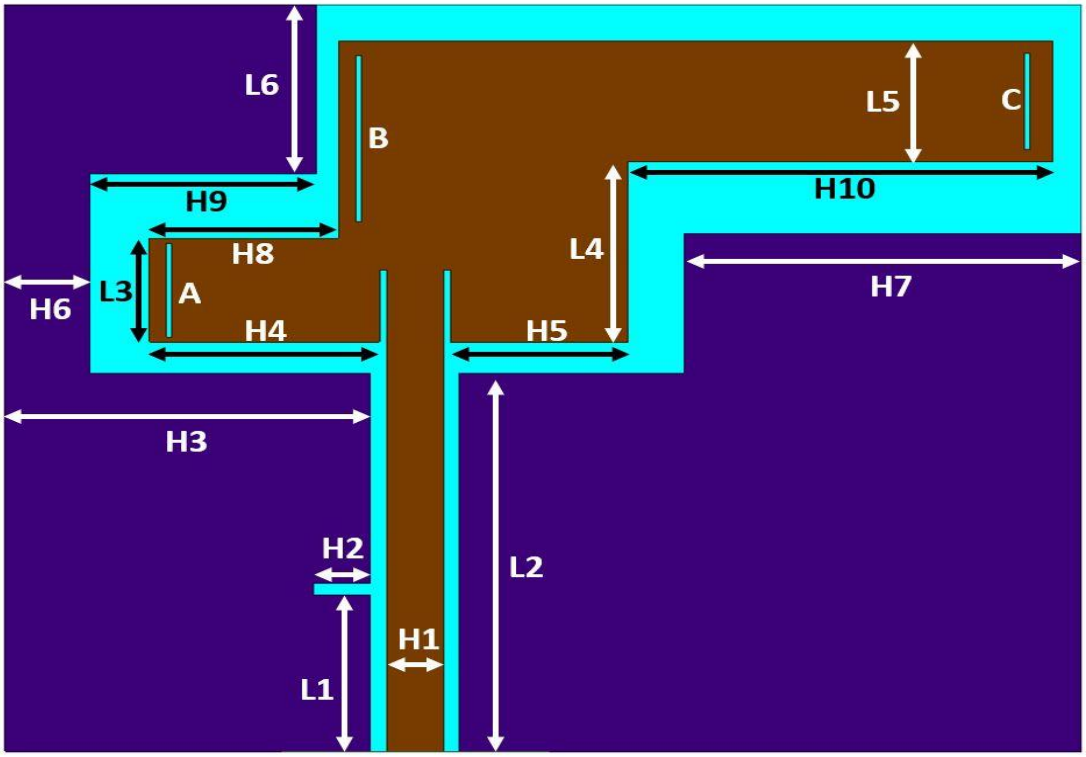

Figure 3.1: Design of the proposed antenna. Values of optimized parameters are: H1 = 2 mm, H2 = 2 mm, H3 = 12.9 mm, H4 = 8.12 mm, H5 = 6.28 mm, H6 = 3 mm, H7 = 14 mm, H8 = 6.67 mm, H9 = 10 mm, H10 = 15 mm, L1 = 6.5 mm, L2 = 15.7 mm, L3 = 4.3 mm, L4 = 7.5 mm, L5 = 5 mm, L6 = 7 mm.

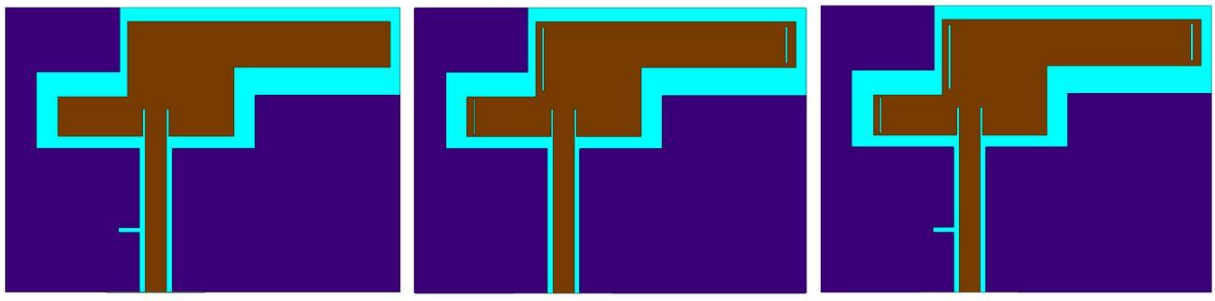

Figure 3.2: Design evolution of the proposed antenna.

Simulated results:

Figure 3.3(a) shows the S11 parameter and Figure 3.3(b) shows the axial ratio of the proposed antenna. With the patch slot only, S11 parameter maintains a bandwidth of 73 MHz from 3.88 GHz to 4.61 GHz. However, ARBW is 20 MHz (4.21 GHz - 4.41 GHz). To increase the ARBW, ground slot is introduced, and patch slot is removed. S11 parameter has a bandwidth of 71 MHz from 3.85 GHz to 4.56 GHz for this case. ARBW increases to 36 MHz from 4.11 GHz to 4.47 GHz. By applying both patch slot and ground slot, ARBW further increases to 45 MHz (4.07 GHz - 4.52 GHz), whereas S11 maintains a bandwidth of 73 MHz from 3.8 GHz to 4.53 GHz. Figure 3.4 shows the peak gain and radiation efficiency of the proposed antenna. The antenna has a radiation efficiency over 91% for our discussed bandwidth. Peak gain is over 3.1 dB from 4.07 GHz to 4.52 GHz. Figure 3.5 shows the simulated radiation pattern for LHCP and RHCP in both XZ ($\phi = 0°$) and YZ ($\phi = 90°$) plane. It is apparent that pattern for LHCP and RHCP are sufficiently separated (exceeding 20 dB) for broadside direction.

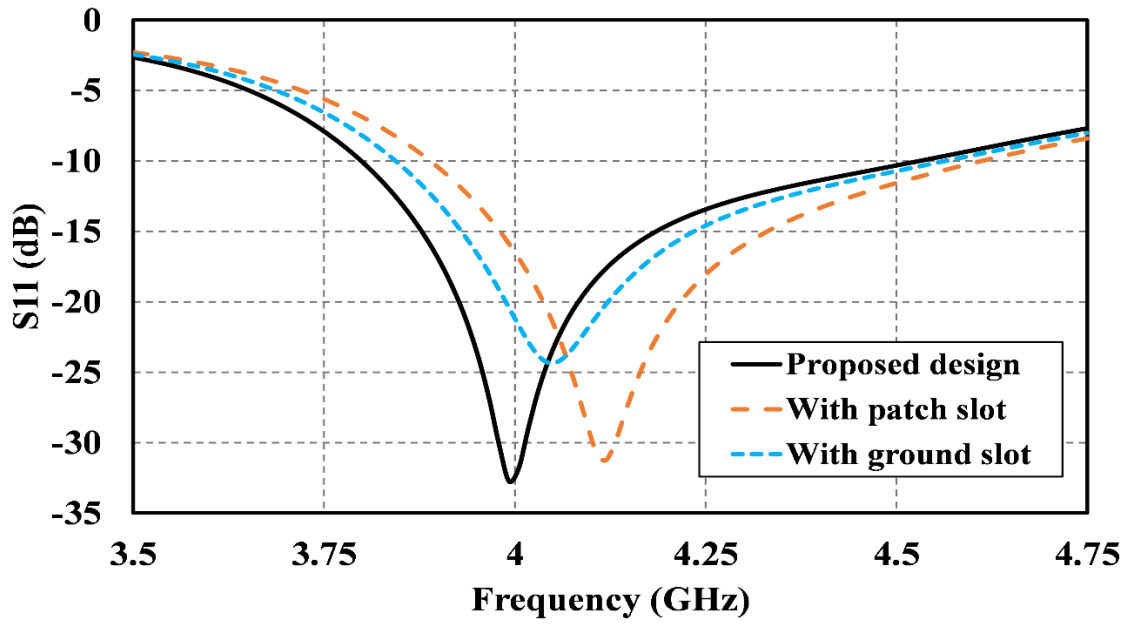

(a)

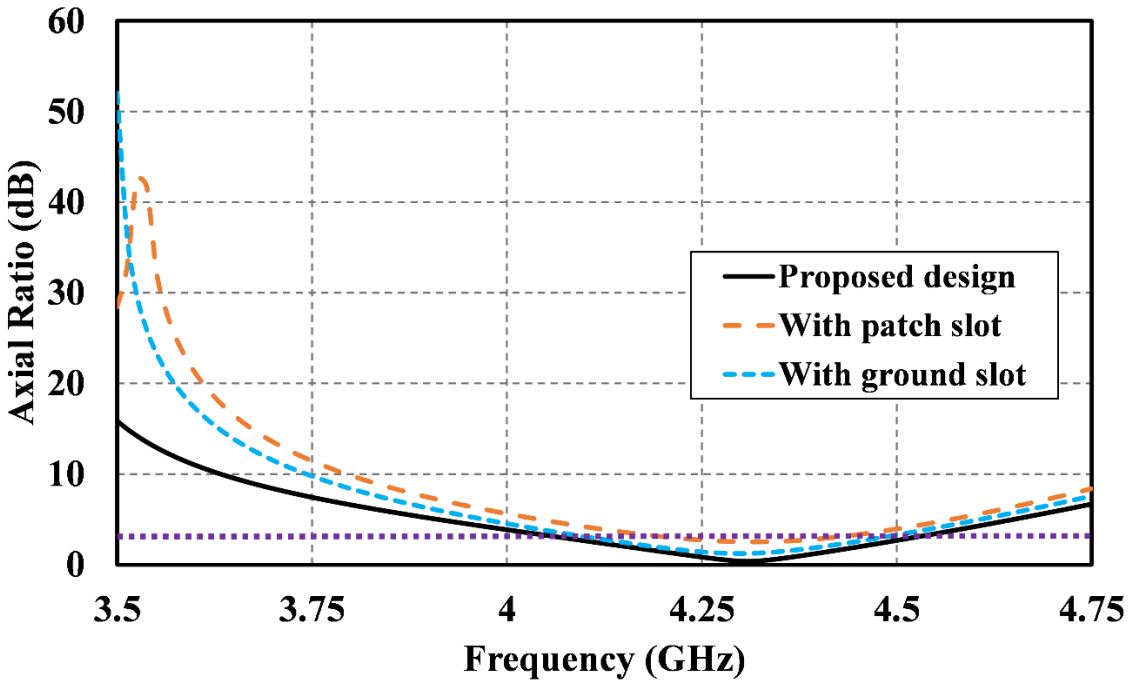

(b)

Figure 3.3: (a) S11 parameter, (b) Axial ratio of the proposed antenna.

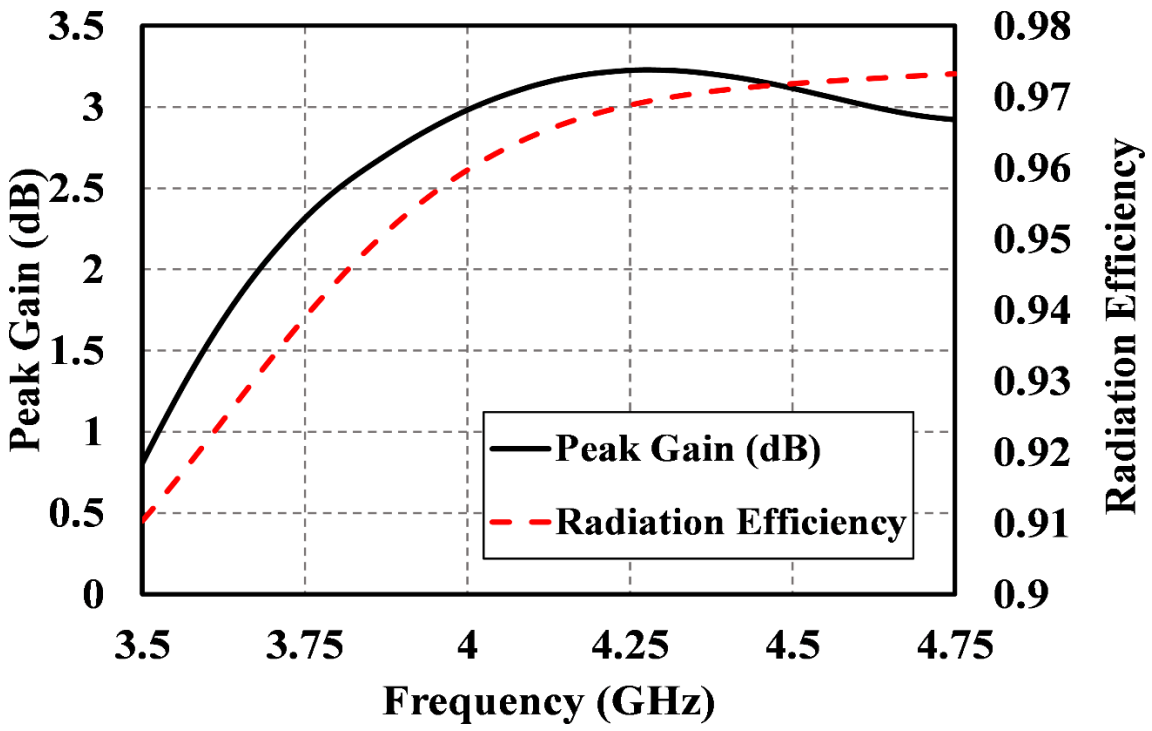

Figure 3.4: Peak gain and radiation efficiency of the proposed antenna.

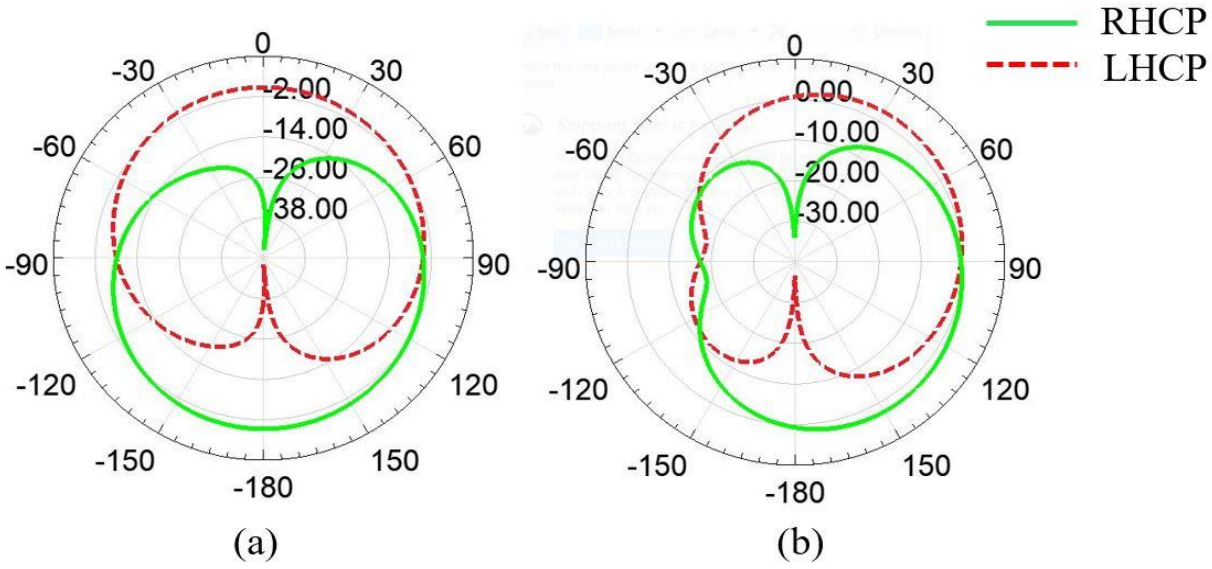

Figure 3.5: Radiation pattern of the antenna at 4.3 GHz, where (a) $\phi = 0°$, (b) $\phi = 90°$. Red line is for LHCP gain and green line is for RHCP gain.

CHAPTER FOUR: INKJET PRINTED FLEXIBLE DUAL BAND CIRCULARLY POLARIZED PATCH ANTENNA

Introduction:

With the advancement of 5G network, internet of things (IOT) devices are flourishing, creating the necessity of developing lightweight, flexible, easily integrable, portable, small size, and easily manufactured antenna systems for better connectivity with the IOT framework. Along with their uses in IOT devices and consumer electronics, flexible antennas can be used in wearable sensors, RFID tags, military applications, and wireless body area networks (WBAN) [53]. Flexible materials like polyethylene terephtalate (PET) paper, liquid crystal polymer (LCP), thin glass, polydimethylsiloxane (PDMS), textile materials (fleece fabrics, denim, cotton, polyster, felt etc.) are employed as substrate while fabricating antenna using inkjet printing, screen printing, 3-d printing, chemical etching and flexography [59], [83]–[86]. For inkjet printing, coplanar waveguide feed (CPW-fed) antennas are best for their simple realization. Researchers have already proposed different CPW-fed antenna on PET paper for different resonance frequencies. In [57], a CPW-fed inkjet printed antenna on PET paper is presented with ultra wide band operating at 3.04 GHZ - 10.70 GHz and 15.18 GHz – 18 GHz, maintaining an average peak gain of 3.94 dB. A CPW-fed bowtie slot wide band antenna is proposed for 2.1 GHz to 4.35 GHz on PET paper [87]. However, these antennas provide linearly polarized (LP) operation, which has disadvantages like increased multipath losses, and signal attenuation due to polarization alignment mismatch of sender and receiver antenna. Circularly polarized (CP) antennas offer improved performance over LP antennas as it radiates two orthogonal electric field vectors with equal magnitudes and one quarter wavelength out of phase. On that account, CP antennas are better suited for flexible and moving devices as they are prone to polarization losses. In[88], a CPW-fed circular polarized

design is proposed for wearable applications for 5.8 GHz. This design has used a thin Rogers substrate layer along with a reflector layer to reduce the loading effect on the human body. This antenna has an 18.3% axial ratio bandwidth (ARBW). Saraswat et al.[45] has proposed another CPW-fed design on polyethylene terephthalate polyester (PETP) film based substrate that has ARBW of 13.49% from 2.35 GHz - 2.69 GHz. A U-shaped slot is cut from the patch while a portion of the ground plane from the left side is taken out to introduce asymmetry to generate circular polarization. Some other flexible circularly polarized antenna is proposed using different feeding techniques, which are summarized concisely in Table 4.1.

In this section, a CPW-fed antenna is proposed on PET paper for CP application with a dual band ARBW of 0.39 GHz and 0.25 GHz. The antenna is optimized, and parameters like reflection coefficient (S11), axial ratio, gain, radiation efficiency, and bending characteristics are simulated based on the finite element method (FEM). A prototype of the designed antenna is fabricated using inkjet printing technology.

Table 4.1: Literature review of flexible circularly polarized antennas.

Reference	Resonance Frequency, GHz	%BW	% AR	Dimensions	Substrate Material	Year
[89]	8.75	34.29%	32.91%	0.47λ x 0.47λ x .0074λ	Taconic, RF-35A2	2015
[47]	2.4	15.9%	2.72%	0.41λ x 0.41λ x .045λ	PDMS & AgNW	2017
[49]	3.59 & 6.3	10.58% & 19.04%	6.96% & 11.11%	0.44λ x 0.37λ x .0016λ	Liquid Crystal Polymer (LCP)	2020
[90]	5.8	6.9%	1.38%	0.52λ x 0.44λ x .0193λ	ROHACELL 71HF& Conductive Graphene Film	2020
[50]	5.8	6.6%	3.85%	0.68λ x 0.68λ x .044λ	Flexible Polymide & Foam	2020
[48]	10.975	28.33%	11.25%	1.83λ x 1.83λ x .0365λ	Woollen Felt	2022
[46]	2.4	14.42%	4.16%	0.24λ x 0.24λ x .0272λ	PDMS	2022
[91]	5.44	43.75%	34%	0.73λ x 0.73λ x .07λ	Polyester Fabric	2022

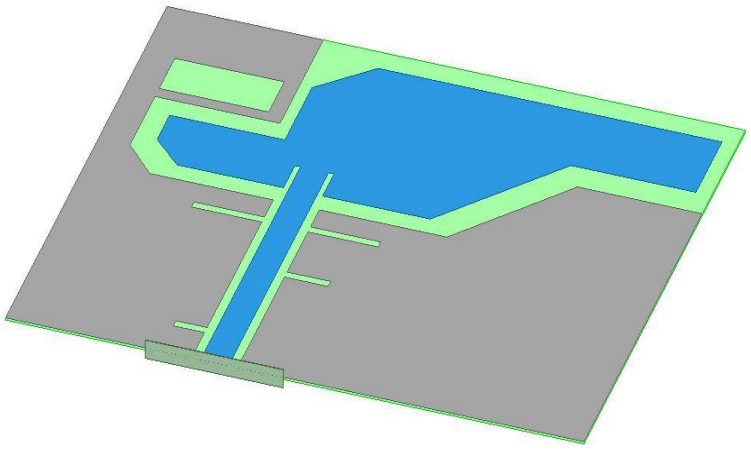

(a)

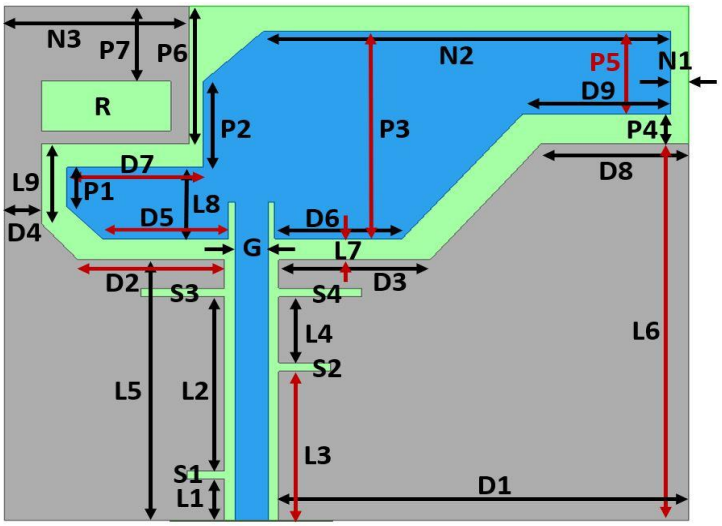

(b)

Figure 4.1: Proposed circularly polarized patch antenna. (a) Trimetric view, (b) Top view with detailed parameter marking.

Antenna Design:

Design Configuration:

The configuration of the proposed antenna is shown in Figure 4.1. The antenna is printed on one side of the commercially available PET paper with a dielectric constant of 3.2, a loss tangent of 0.022, and a thickness of 0.135mm. PET paper is very light, cheap, flexible with adequate rigidity, and inkjet printer friendly, making it useful as a substrate for low cost and simple antenna design. The dimension of the antenna is 31 mm x 37 mm. The patch of the antenna is modified "S" shape, which is inset-fed by a 50Ω CPW feed line. The dimension of inset feeding is 2.2 mm X 0.35 mm. The ground plane has slots on both sides of the feed line. These slots are marked as S1 and S3 on the left side and S2 and S4 on the right side. All slots are 0.5 mm wide. The lengths of S1, S2, S3, and S4 are 2 mm, 2.8 mm, 4.5 mm, and 4.5 mm, respectively. The ground plane also has a rectangular cut in the upper left portion, which increases the ARBW slightly along with

reducing the amount of ink needed to print the antenna. The dimension of the rectangular cut is 7 mm x 3 mm. The structure of the antenna is simulated and optimized by ANSYS HFSS. The optimized parameters of the antenna are given in Table 4.2.

Table 4.2: Optimized parameters of the proposed antenna.

Parameter	**Value, mm**	**Parameter**	**Value, mm**
L1	2.5	D1	22.16
L2	10.5	D2	7.9
L3	9	D3	8.16
L4	4	D4	2
L5	15.7	D5	6.82
L6	22.7	D6	6.88
L7	1.3	D7	7.37
L8	4.3	D8	8
L9	4.8	D9	8
P1	2.4	P6	8.3
P2	5.19	P7	4
P3	12.5	N1	1
P4	1.8	N2	22
P5	5	N3	10

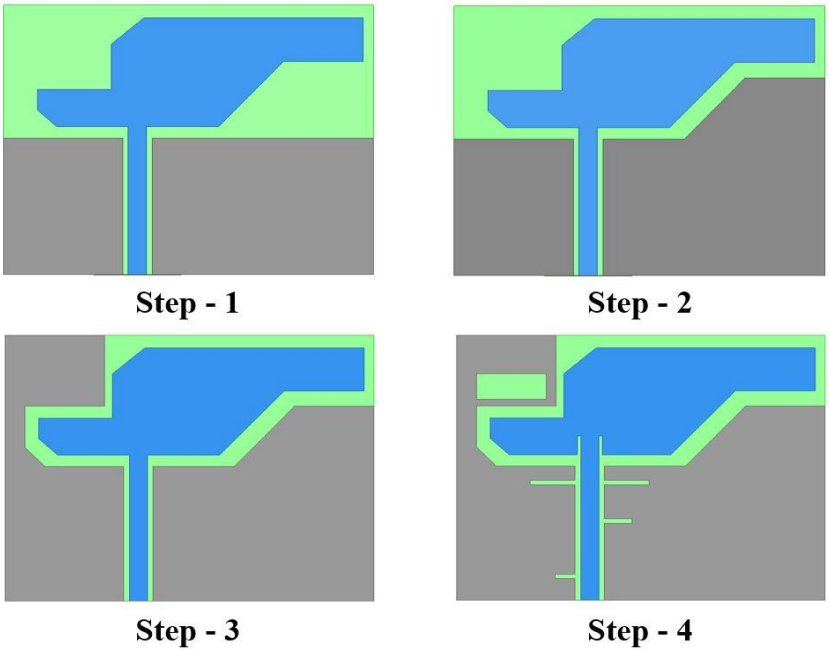

Figure 4.2: Evolution of the patch and the ground of the proposed antenna.

Design Steps of the Antenna:

The evolution of the design is shown in Figure 4.2. Primarily, the antenna is designed by putting the modified S-shaped patch over the feedline. The upper-right portion of the shape is more extended outwards to create asymmetry in the design. The feed line is shifted to the left side to create space for the ground plane to cover the extended right side portion of the patch. This design shows a bandwidth of 1.05 GHz (6.75 GHz - 7.8 GHz) and an ARBW of 0.52 GHz (4.8 GHz -5.32 GHz). However, as bandwidths are not overlapping, the antenna will not work as a CP antenna. The symmetry of the ground plane is broken by placing a trapezium over the right side, as it is a useful way to generate circular polarization. This makes the antenna work on dual band with bandwidths of 0.42 GHz (4.54 GHz - 4.96 GHz) and 1.14 GHz (6.78 GHz - 7.92 GHz). Nonetheless, no ARBW is observed in this case. After that, the ground plane is extended upwards on the left side by shielding the elongated left part of the “S” shaped patch. This modification doubles the bandwidth of the first band (4.09 GHz - 5.07 GHz) while shifting and slightly

decreasing the bandwidth (7.17 GHz - 8.2 GHz) of the second band on the right side. More importantly, the antenna shows an overlapping ARBW of 0.36 GHz (4.32 GHz - 4.68 GHz) with the return loss. Finally, two slots on each side of the ground plane along the feed line are introduced along with inset feeding and a rectangular cut in the upper left corner of the ground plane. This results in shifting the second band to 6.23 GHz (bandwidth 1.35 GHz) while the first band remains almost similar position with the bandwidth of 1.04 GHz (4.01 GHz - 5.05 GHz). Moreover, an ARBW of 0.25 GHz (7.11 GHz - 7.36 GHz) is observed in the second band, along with an ARBW of 0.39 GHz (4.23 GHz - 4.62 GHz) in the first band. Figure 4.3 shows the S11 and axial ratio with respect to frequency according to the steps described above.

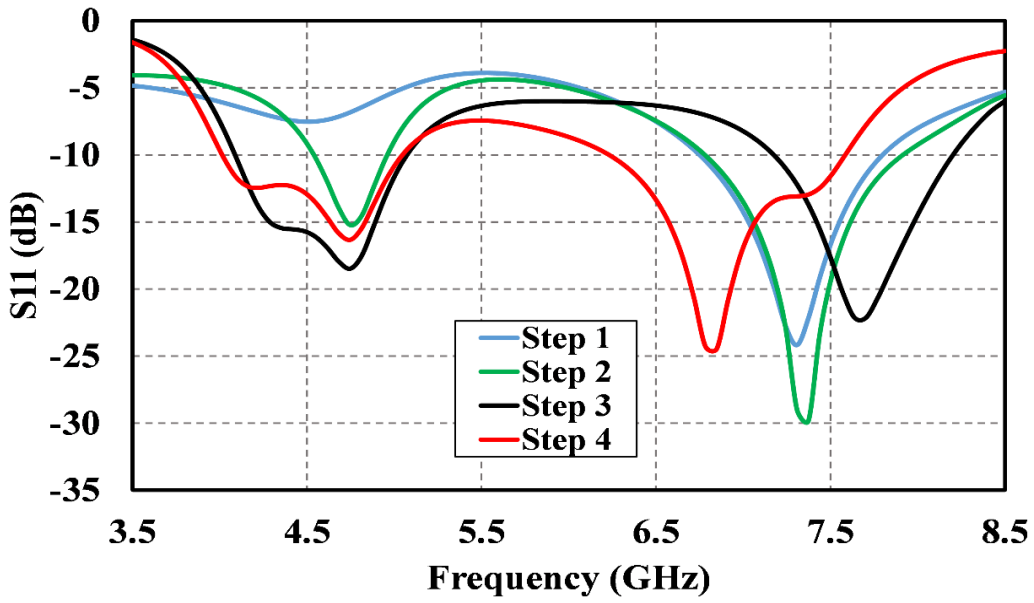

(a)

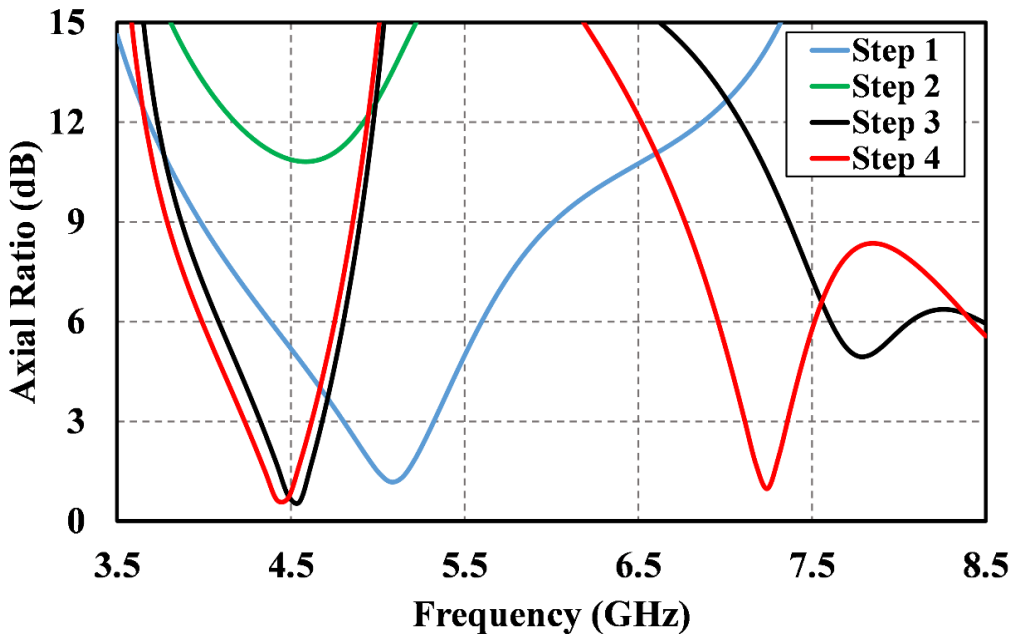

(b)

Figure 4.3: Simulated parameters for different patch design steps. (a) S11, (b) Axial Ratio.

Radiation Efficiency, Gain, and Radiation Pattern Analysis:

Figure 4.4 shows the peak gain and radiation efficiency of the antenna as a function of frequency. The average peak gain over the frequency range is around 3.35 dB while the lowest peak gain is 2.88 dB at 4.95 GHz and highest peak gain is 3.63 dB at 4.42 GHz in the first working band. In the second working band, average peak gain is around 3.5 dB while the lowest and highest peak gain is 3.11 dB and 4.14 dB respectively. The gain shows an increasing trend towards high frequency as antenna's electrical size increases. The average radiation efficiency is over 97% in the first band while it decreases to 96% in the second band. In Figure 4.5, simulated far field radiation patterns of LHCP and RHCP gain is observed in both xz (E-plane) and yz (H-plane) plane for 4.5 GHZ and 7.25 GHz. At 4.5 GHz, LHCP is observed in at +Z direction and RHCP is

observed in -Z direction for both xz and yz plane. However, at 7.25 GHz LHCP and RHCP is observed at -Z and +Z direction respectively for both planes.

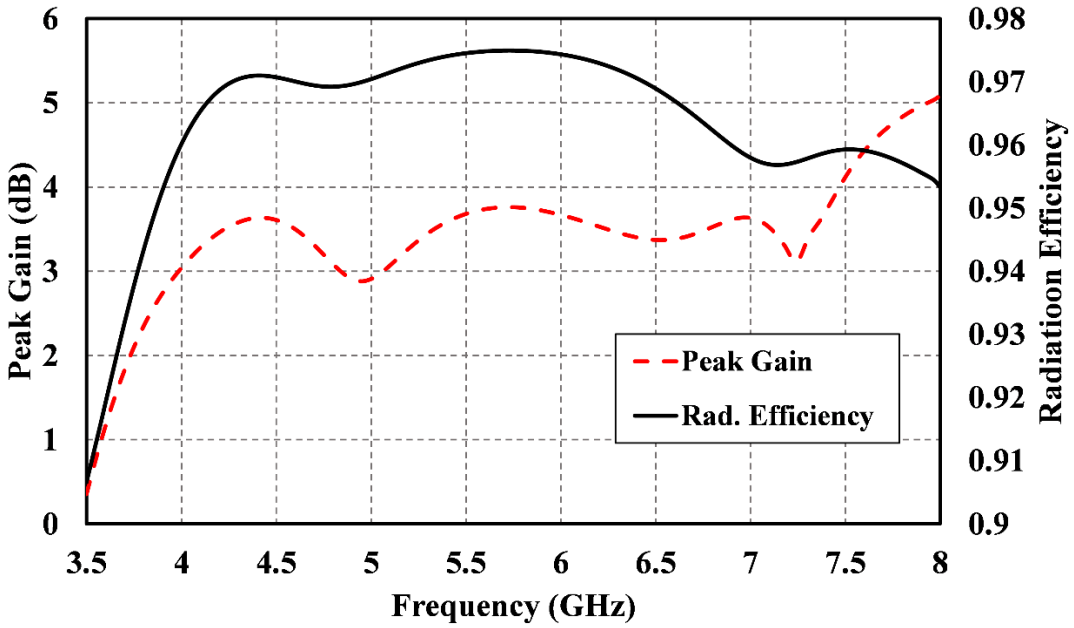

Figure 4.4: Simulated peak gain and radiation efficiency of the proposed antenna.

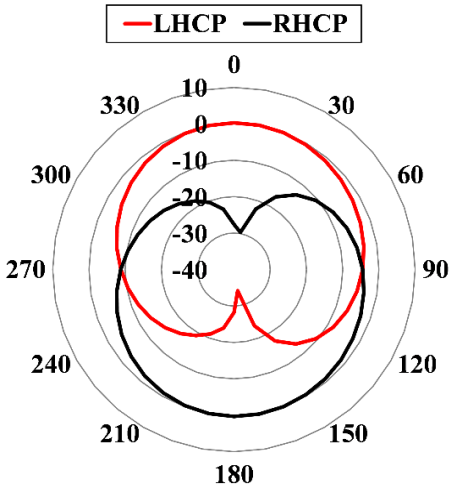

(a)

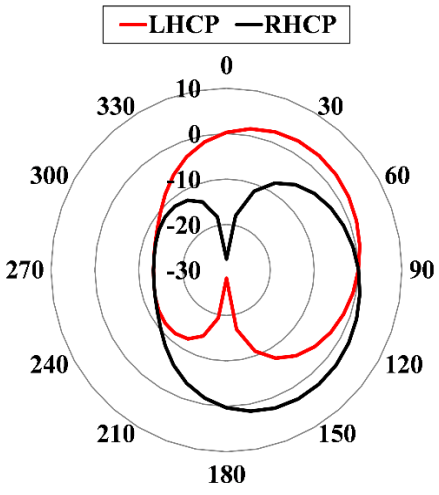

(b)

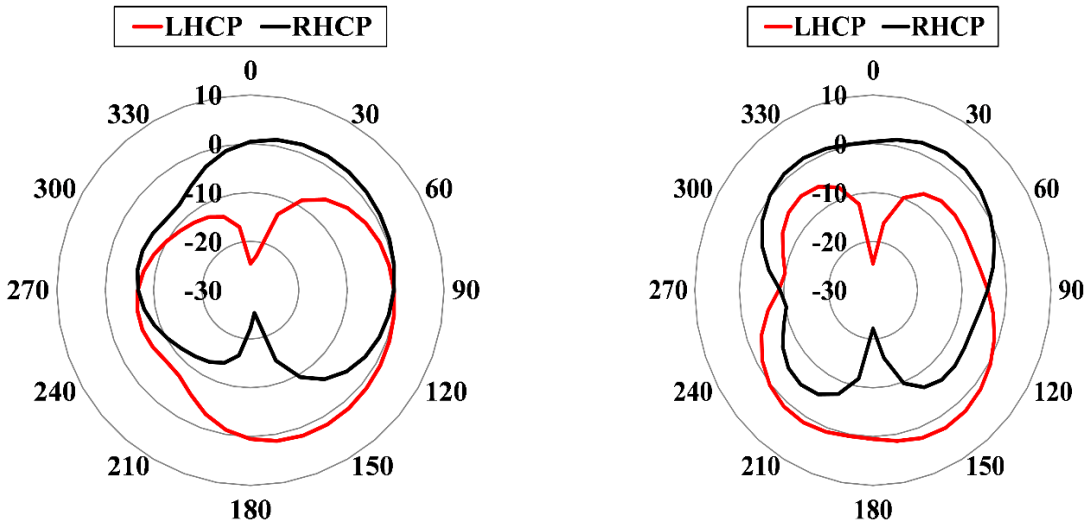

(c) (d)

Figure 4.5: Simulated radiation pattern of LHCP and RHCP gain for frequency 4.5 GHz (a) xz plane, (b) yz plane, and for frequency 7.25 GHz (c) xz plane, (d) yz plane.

Result and Discussion:

The optimized version of the antenna is printed using a Fujifilm Dimatix 2831 inkjet printer (DMP). Silver nanoparticle ink (JS-A-102A) from Novacentrix is used for printing the antenna using a Fujifilm Samba cartridge. The antenna is printed double layer to ensure high conductivity. After that, the antenna is sintered in a hotplate, gradually increasing the temperature from 90°C to 140°C. Temperature is increased in three steps with a total sintering time of 1 hour. The fabricated antenna is tested using Keysight Fieldfox N9952A microwave analyzer. Figure 4.6 shows the printed antenna and the measurement using a network analyzer.

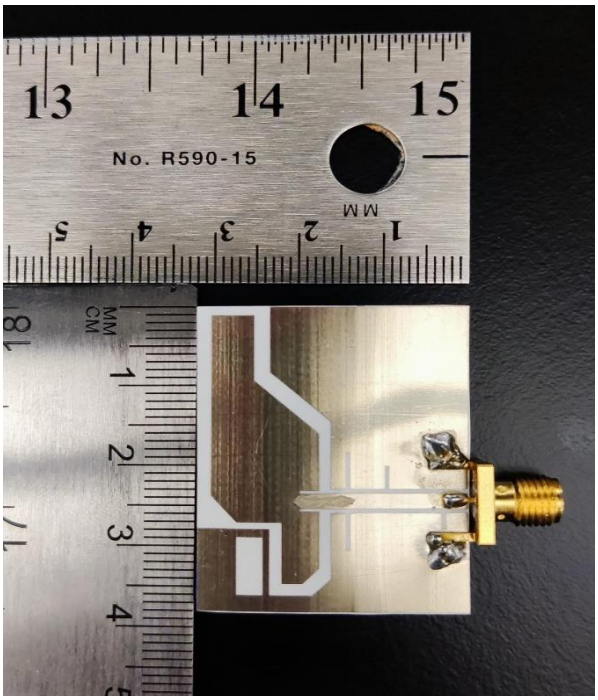

(a)

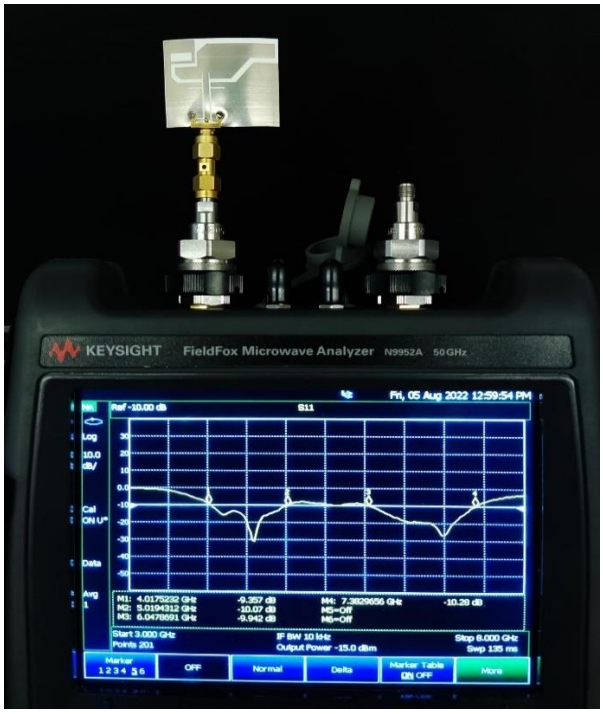

(b)

Figure 4.6: (a) Fabricated antenna, (b) Antenna measurement.

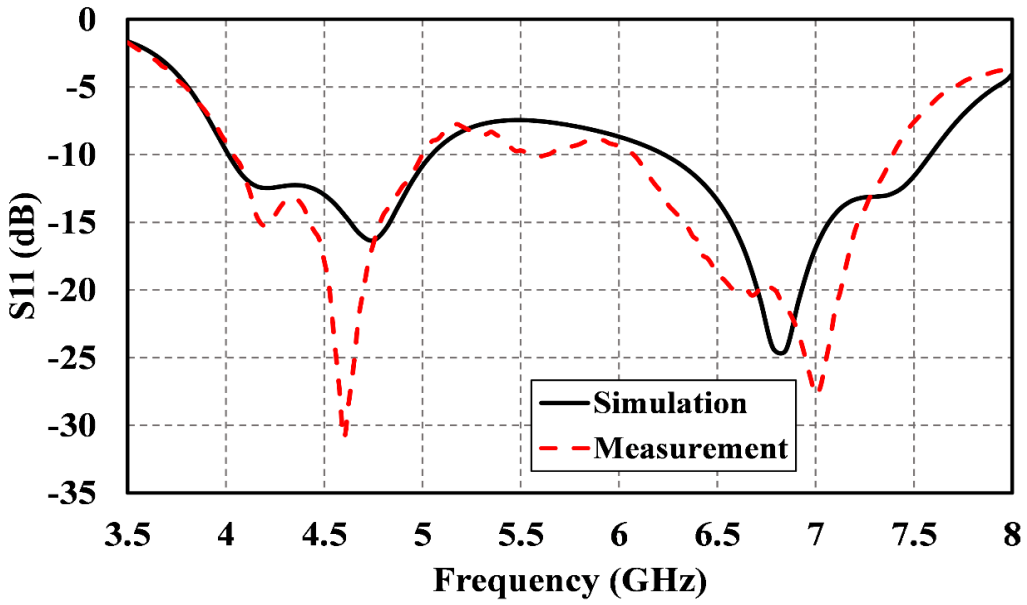

Figure 4.7: Comparison of simulated and measured S11 parameter.

Figure 4.7 shows the comparison of S11 simulation and measurement. It is noted that the simulated antenna has two resonance points at 4.22 GHz and 4.75 GHz in the first band. Measured data shows resonance points at 4.2 GHz and 4.6 GHz. However, the bandwidth matches almost exactly, starting from 4.04 GHz to 4.98 GHz. For the second band, the resonance point in the measurement shifts to 7 GHz while it is at 6.85 GHz in the simulation data. Though the resonance point shift to the right side, the antenna band shifts to the left side, starting at 6.075 GHz and ending at 7.375 GHz. The reason for these minor discrepancies is inherent imperfections in printing, connector matching loss, and the effect of the measuring environment. As the antenna is flexible, it is necessary to check its robustness of the antenna by examining it for different bending conditions. Figure 4.8 demonstrates that the antenna is examined under vertical and horizontal bending conditions. For both cases, the antenna shows similar pattern like the flat condition, which is presented in Figure 4.9. So, it can be noted that the bending conditions do not meaningfully affect the performance of the antenna.

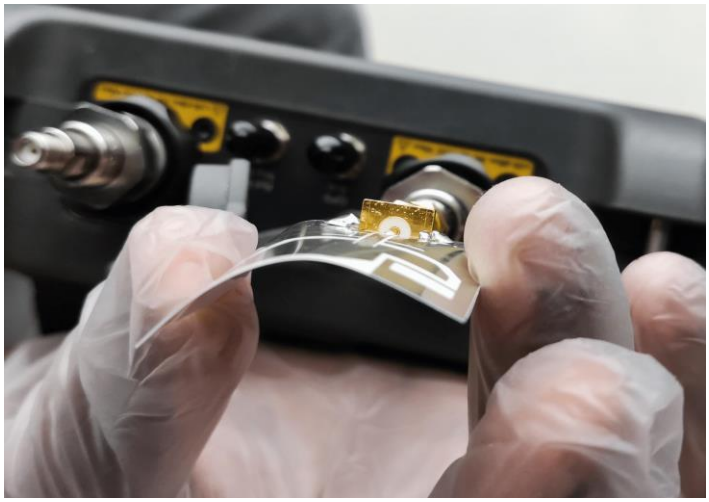

(a)

(b)

Figure 4.8: Images of fabricated antenna bending. (a) Horizontal bending, (b) Vertical bending.

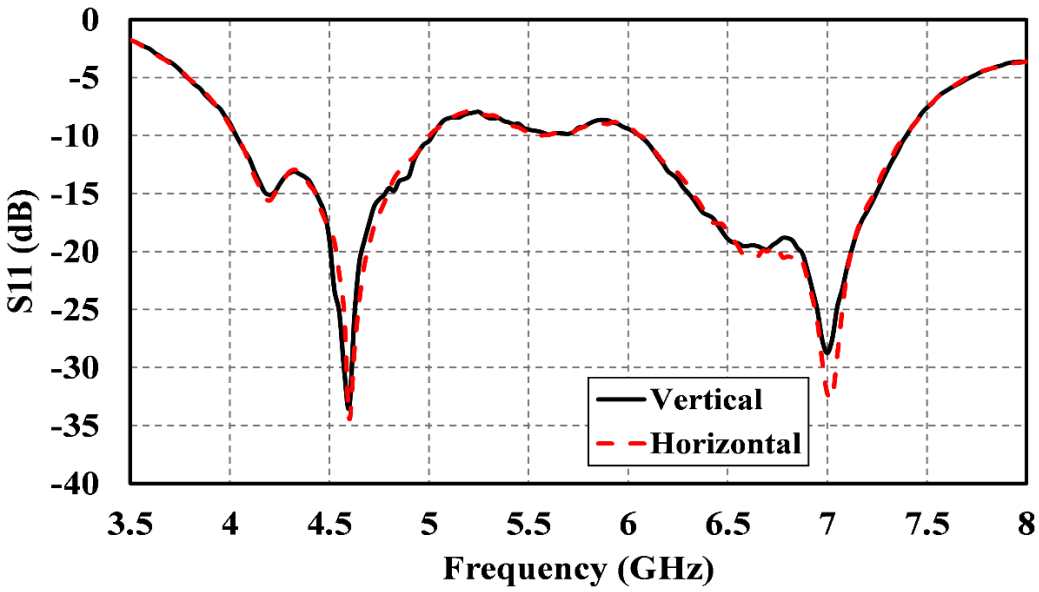

Figure 4.9: Measured S11 parameter for horizontal and vertical bending.

CHAPTER FIVE: CONCLUSION

The objective of this thesis is to develop flexible inkjet printed antennas for specific purposes like full duplex application and circular polarization application. The antennas are firstly designed and optimized in HFSS, and after that, they are fabricated and characterized to match the simulation results. In the first design, a flexible full duplex antenna is proposed on PET paper for 5.8 GHz wearable applications. Inset feeding and corner cut along with DGS are introduced to implement -50 dB isolation on the resonant frequency with around 220 MHz bandwidth. The antenna can be fabricated easily using inkjet printing on PET paper which is glued with the foam layer using glue afterward. Bending tests and on body characterization are performed on the fabricated antenna. Antenna shows desired performance in all the experiments making it a robust performer. It also provides high gain, high radiation efficiency, and low SAR level, making it a suitable candidate for full duplex wearable applications. For my second work, a flexible CP antenna is proposed for applications in C band. Wider ARBW is achieved by using slots in patch and ground, while making it simple for fabrication and integration with other circuits by applying CPW-feeding. As the antenna is designed on a fully flexible material, it will be useful for any applications that require structural flexibility. An improvement of the second work is proposed as the final work of this thesis. A flexible circularly polarized antenna is proposed on PET paper for dual band CP application. The antenna is designed as a CPW-fed antenna with a modified “S” shape patch with multiple slots in the ground plane. This antenna is compact, simple, cheap, and lightweight, along with its robustness towards bending applications. By studying different parameters like S11, axial ratio, gain, radiation efficiency, and radiation pattern, it can be summarized that this antenna is a great solution to consider for 4.23 GHz - 4.62 GHz and 7.11 GHz - 7.36 GHz circularly polarized applications.

There is a wide scope of improvements in these projects as future works. Firstly, full duplex antenna can be made more optimized and compact. Also, there are certain other bandwidths for which designs can also be explored. Secondly, an interesting work can also be the development of flexible full duplex antennas for circular polarization applications, as both are highly unexplored fields.

REFERENCES

[1] A. Sabharwal, P. Schniter, D. Guo, D. W. Bliss, S. Rangarajan, and R. Wichman, "In-Band Full-Duplex Wireless: Challenges and Opportunities," *IEEE Journal on Selected Areas in Communications*, vol. 32, no. 9, pp. 1637–1652, Sep. 2014, doi: 10.1109/JSAC.2014.2330193.

[2] Z. Zhang, X. Chai, K. Long, A. V. Vasilakos, and L. Hanzo, "Full duplex techniques for 5G networks: self-interference cancellation, protocol design, and relay selection," *IEEE Communications Magazine*, vol. 53, no. 5, pp. 128–137, May 2015, doi: 10.1109/MCOM.2015.7105651.

[3] D. Bharadia, E. McMilin, and S. Katti, "Full duplex radios," *SIGCOMM Comput. Commun. Rev.*, vol. 43, no. 4, pp. 375–386, Aug. 2013, doi: 10.1145/2534169.2486033.

[4] C. D. Nwankwo, L. Zhang, A. Quddus, M. A. Imran, and R. Tafazolli, "A Survey of Self-Interference Management Techniques for Single Frequency Full Duplex Systems," *IEEE Access*, vol. 6, pp. 30242–30268, 2018, doi: 10.1109/ACCESS.2017.2774143.

[5] H. Nawaz and I. Tekin, "Dual polarized patch antenna with high inter-port isolation for 1GHz in-band full Duplex applications," in *2016 IEEE International Symposium on Antennas and Propagation (APSURSI)*, Jun. 2016, pp. 2153–2154. doi: 10.1109/APS.2016.7696783.

[6] T. J. Douglas and K. Sarabandi, "Planar antenna system for full-duplex applications," in *2017 XXXIInd General Assembly and Scientific Symposium of the International Union of Radio Science (URSI GASS)*, Aug. 2017, pp. 1–3. doi: 10.23919/URSIGASS.2017.8105210.

[7] J.-F. Li, D.-L. Wu, G. Zhang, Y.-J. Wu, and C.-X. Mao, "Compact Dual-Polarized Antenna for Dual-Band Full-Duplex Base Station Applications," *IEEE Access*, vol. 7, pp. 72761–72769, 2019, doi: 10.1109/ACCESS.2019.2918982.

[8] X.-J. Lin, Z.-M. Xie, and P.-S. Zhang, "Integrated Filtering Microstrip Duplex Antenna Array with High Isolation," *International Journal of Antennas and Propagation*, vol. 2017, p. e4127943, Feb. 2017, doi: 10.1155/2017/4127943.

[9] H. Nawaz, Ö. Gürbüz, and I. Tekin, "High isolation slot coupled antenna with integrated tunable self-interference cancellation circuitry," *Electronics Letters*, vol. 54, no. 23, pp. 1311–1312, 2018, doi: 10.1049/el.2018.6644.

[10] A. A. Jasim, K. H. Sayidmarie, R. A. Abd-Alhameed, and A. Ali, "Integrated antenna technique for cancelling the self-interference signal in full-duplex communication," *PIER C*, vol. 97, pp. 43–55, 2019, doi: 10.2528/PIERC19081902.

[11] H. Nawaz, A. U. Niazi, and S. M. Chaudhry, "High isolation, proximity-fed monostatic patch antennas with integrated self-interference cancellation-taps for ISM band full duplex applications," *International Journal of RF and Microwave Computer-Aided Engineering*, vol. 31, no. 1, p. e22484, 2021, doi: 10.1002/mmce.22484.

[12] G. Chaudhary, J. Jeong, Y. Jeong, and W. Ham, 2020. "Microstrip antenna with high self-interference cancellation using phase reconfigurable feeding network for in-band full duplex communication," Microwave and Optical Technology Letters, 62(2), pp.919-925.

[13] J. M. Laco, F. H. Gregorio, G. González, J. E. Cousseau, T. Riihonen, and R. Wichman, "Patch antenna design for full-duplex transceivers," in *2017 European Conference on Networks and Communications (EuCNC)*, Jun. 2017, pp. 1–5. doi: 10.1109/EuCNC.2017.7980704.

[14] Y.-M. Zhang and J.-L. Li, "A Dual-Polarized Antenna Array With Enhanced Interport Isolation for Far-Field Wireless Data and Power Transfer," *IEEE Transactions on Vehicular Technology*, vol. 67, no. 11, pp. 10258–10267, Nov. 2018, doi: 10.1109/TVT.2018.2865415.

[15] D. Wójcik, M. Surma, A. Noga, and M. Magnuski, "High Port-to-Port Isolation Dual-Polarized Antenna Array Dedicated for Full-Duplex Base Stations," *IEEE Antennas and Wireless Propagation Letters*, vol. 19, no. 7, pp. 1098–1102, Jul. 2020, doi: 10.1109/LAWP.2020.2989698.

[16] K. Gbafa, A. Diallol, P. L. Thuc, and R. Staraj, "Tx/Rx Antenna System for Full-Duplex Application," in *2018 IEEE International Symposium on Antennas and Propagation & USNC/URSI National Radio Science Meeting*, Jul. 2018, pp. 1571–1572. doi: 10.1109/APUSNCURSINRSM.2018.8608497.

[17] Y.-M. Zhang, S. Zhang, J.-L. Li, and G. F. Pedersen, "A Dual-Polarized Linear Antenna Array With Improved Isolation Using a Slotline-Based 180° Hybrid for Full-Duplex Applications," *IEEE Antennas and Wireless Propagation Letters*, vol. 18, no. 2, pp. 348–352, Feb. 2019, doi: 10.1109/LAWP.2019.2890983.

[18] T. J. Douglas and K. Sarabandi, “Compact Planar Antenna System for Full- Duplex Wireless Applications,” in *2018 IEEE International Symposium on Antennas and Propagation & USNC/URSI National Radio Science Meeting*, Jul. 2018, pp. 1303–1304. doi: 10.1109/APUSNCURSINRSM.2018.8609281.

[19] S. Chaudhuri, R. S. Kshetrimayum, and R. Kumar Sonkar, “High Inter-port Isolation Dual Circularly Polarized Modified Franklin Microstrip Antenna,” in *2019 13th European Conference on Antennas and Propagation (EuCAP)*, Mar. 2019, pp. 1–4.

[20] Y.-M. Zhang and J.-L. Li, “Differential-Series-Fed Dual-Polarized Traveling-Wave Array for Full-Duplex Applications,” *IEEE Transactions on Antennas and Propagation*, vol. 68, no. 5, pp. 4097–4102, May 2020, doi: 10.1109/TAP.2019.2948393.

[21] “Patch antennas with ring hybrid feeding structures and defected ground structure for full-duplex applications - Washington State University.” https://rex.libraries.wsu.edu/esploro/outputs/graduate/Patch-antennas-with-ring-hybrid-feeding/99900525198401842 (accessed Oct. 25, 2022).

[22] H. Nawaz and I. Tekin, “Dual-Polarized, Differential Fed Microstrip Patch Antennas With Very High Interport Isolation for Full-Duplex Communication,” *IEEE Transactions on Antennas and Propagation*, vol. 65, no. 12, pp. 7355–7360, Dec. 2017, doi: 10.1109/TAP.2017.2765829.

[23] H. Nawaz and I. Tekin, “Three ports microstrip patch antenna with dual linear and linear co-polarisation characteristics,” *Electronics Letters*, vol. 53, no. 8, pp. 518–520, 2017, doi: 10.1049/el.2016.2923.

[24] H. Nawaz and I. Tekin, “Double-Differential-Fed, Dual-Polarized Patch Antenna With 90 dB Interport RF Isolation for a 2.4 GHz In-Band Full-Duplex Transceiver,” *IEEE Antennas and Wireless Propagation Letters*, vol. 17, no. 2, pp. 287–290, Feb. 2018, doi: 10.1109/LAWP.2017.2786942.

[25] G. Makar, D. Kim, N. Tran, and T. Karacolak, “compact antennas with reduced self interference for simultaneous transmit and receive,” *PIER C*, vol. 78, pp. 19–31, 2017, doi: 10.2528/PIERC17051205.

[26] C. Goodbody, T. Karacolak, and N. Tran, “Dual-polarised patch antenna for in-band full duplex applications,” *Electronics Letters*, vol. 54, no. 22, pp. 1255–1256, 2018, doi: 10.1049/el.2018.5324.

[27] H. Nawaz and M. A. Basit, “Single layer, dual polarized, 2.4 GHz patch antenna with very high rf isolation between dc isolated tx-rx ports for full duplex radio,” *PIER Letters*, vol. 85, pp. 65–72, 2019, doi: 10.2528/PIERL19032806.

[28] S. Khaledian, F. Farzami, B. Smida, and D. Erricolo, “Robust Self-Interference Cancellation for Microstrip Antennas by Means of Phase Reconfigurable Coupler,” *IEEE Transactions on Antennas and Propagation*, vol. 66, no. 10, pp. 5574–5579, Oct. 2018, doi: 10.1109/TAP.2018.2860623.

[29] H. Nawaz, N. Shoaib, A. U. Niazi, and S. M. Chaudhry, 2021. “A compact, bistatic antenna system with very high interport isolation for 2.4 GHz in-band full duplex applications,” International Journal of Antennas and Propagation, 2021.

[30] H. Nawaz, A. U. Niazi, M. A. Basit, F. Shaukat, and M. Usman, “Dual-polarized, monostatic antenna array with improved Tx–Rx isolation for 2.4 GHz in-band full duplex applications,” *International Journal of Microwave and Wireless Technologies*, vol. 12, no. 5, pp. 398–408, Jun. 2020, doi: 10.1017/S1759078719001569.

[31] J. Lu, C. Gu, and J.-F. Mao, “A 5.8GHz ISM Band Single Antenna with Coupling Structure for Full-Duplex Doppler Radar Sensing,” in *2020 IEEE MTT-S International Wireless Symposium (IWS)*, Sep. 2020, pp. 1–3. doi: 10.1109/IWS49314.2020.9360205.

[32] T. Nguyen and T. Karacolak, “Planar patch antenna system with high isolation for full-duplex applications,” *Electronics Letters*, vol. 55, no. 25, pp. 1326–1329, 2019, doi: 10.1049/el.2019.3059.

[33] S. Piramasubramanian, M. G. Madhan, and S. Gopikasri, “Dual Port Dual Polarized Patch Antenna with Integrated Defected Ground Structure for 2.5 GHz In - Band Full Duplex Application,” in *2019 IEEE 1st International Conference on Energy, Systems and Information Processing (ICESIP)*, Jul. 2019, pp. 1–4. doi:10.1109/ICESIP46348.2019.8938368.

[34] C. Goodbody, N. Tran, and T. Karacolak, “Patch antenna for full duplex application with improved isolation using defected ground structure,” *PIER Letters*, vol. 84, pp. 91–97, 2019, doi: 10.2528/PIERL19031808.

[35] G. Chaudhary, J. Jeong, P. Pech, P. Kim, and Y. Jeong, "High Self-Interference Cancellation Antenna for In-Band Full Duplex Communication System," in *2019 49th European Microwave Conference (EuMC)*, Oct. 2019, pp. 236–239. doi:10.23919/EuMC.2019.8910915.

[36] A. H. Hussein, H. H. Abdullah, M. A. Attia, and A. M. Abada, "S-Band Compact Microstrip Full-Duplex Tx/Rx Patch Antenna With High Isolation," *IEEE Antennas and Wireless Propagation Letters*, vol. 18, no. 10, pp. 2090–2094, Oct. 2019, doi: 10.1109/LAWP.2019.2937769.

[37] M.A. Abdalla, and A.M. Abdelraheem, 2017. "Compact transmit receive hybrid electromagnetic isolation in antenna array transceiver system for full duplex applications, " IET Microwaves, Antennas & Propagation, 11(3), pp.417-425.

[38] H. Zhai, D. Yang, L. Xi, and D. Feng, "A new CPW-fed broadband circularly polarized printed monopole antenna for UWB application," *Microwave and Optical Technology Letters*, vol. 60, no. 2, pp. 364–369, 2018, doi: 10.1002/mop.30972.

[39] T. Tuan Le, H. H. Tran, and H. C. Park, "A simple penta-band circularly polarized cpw-fed monopole-patch antenna covering six commercial application bands," *Microwave and Optical Technology Letters*, vol. 60, no. 3, pp. 773–778, 2018, doi: 10.1002/mop.31046.

[40] Q. Chen, H. Zhang, L.-C. Yang, B. Xue, and X.-L. Min, "Broadband cpw-fed circularly polarized planar monopole antenna with inverted-l strip and asymmetric ground plane for wlan application," *PIER C*, vol. 74, pp. 91–100, 2017, doi: 10.2528/PIERC17021203.

[41] B. Mekimah, T. Djerafi, A. Messai, and A. Belhedri, "Broadband circularly polarized cpw fed asymmetrically-shaped slot patch antenna for x band applications," *PIER Letters*, vol. 91, pp. 137–143, 2020, doi: 10.2528/PIERL20042504.

[42] M. Midya, S. Bhattacharjee, and M. Mitra, "Compact cpw-fed circularly polarized antenna for wlan application," *PIER M*, vol. 67, pp. 65–73, 2018, doi: 10.2528/PIERM18021505.

[43] M. Midya, S. Bhattacharjee, and M. Mitra, "Cpw-fed dual-band dual-sense circularly polarized antenna for wimax application," *PIER Letters*, vol. 81, pp. 113–120, 2019, doi: 10.2528/PIERL18091306.

[44] A. Birwal, S. Singh, B. K. Kanaujia, and S. Kumar, "Cpw-fed ultra-wideband dual-sense

circularly polarized slot antenna," *PIER C*, vol. 94, pp. 219–231, 2019, doi: 10.2528/PIERC19052005.

[45] K. Saraswat and A. R. Harish, "Flexible dual-band dual-polarised CPW-fed monopole antenna with discrete-frequency reconfigurability," *IET Microwaves, Antennas & Propagation*, vol. 13, no. 12, pp. 2053–2060, 2019, doi: 10.1049/iet-map.2018.5711.

[46] A. S. M. Sayem *et al.*, "Flexible and Transparent Circularly Polarized Patch Antenna for Reliable Unobtrusive Wearable Wireless Communications," *Sensors*, vol. 22, no. 3, Art. no. 3, Jan. 2022, doi: 10.3390/s22031276.

[47] Z. H. Jiang, Z. Cui, T. Yue, Y. Zhu, and D. H. Werner, "Compact, Highly Efficient, and Fully Flexible Circularly Polarized Antenna Enabled by Silver Nanowires for Wireless Body-Area Networks," *IEEE Transactions on Biomedical Circuits and Systems*, vol. 11, no. 4, pp. 920 932, Aug. 2017, doi: 10.1109/TBCAS.2017.2671841.

[48] H. Arun and I. Govindanarayanan, "Circularly polarized semicircle-shaped flexible bidirectional antenna for X-band RFID applications," *Appl. Phys. A*, vol. 128, no. 8, p. 721, Jul. 2022, doi: 10.1007/s00339-022-05884-4.

[49] M. Venkateswara Rao, B. T. P. Madhav, T. Anilkumar, and B. Prudhvinadh, "Circularly polarized flexible antenna on liquid crystal polymer substrate material with metamaterial loading," *Microwave and Optical Technology Letters*, vol. 62, no. 2, pp. 866–874, 2020, doi: 10.1002/mop.32088.

[50] H. C. Yang, X. Y. Liu, Y. Fan, and M. M. Tentzeris, "Flexible circularly polarized antenna with axial ratio bandwidth enhancement for off-body communications," *IET Microwaves, Antennas & Propagation*, vol. 15, no. 7, pp. 754–767, 2021, doi: 10.1049/mia2.12081.

[51] G. Makar, N. Tran, and T. Karacolak, "A High-Isolation Monopole Array With Ring Hybrid Feeding Structure for In-Band Full-Duplex Systems," *IEEE Antennas and Wireless Propagation Letters*, vol. 16, pp. 356–359, 2017, doi: 10.1109/LAWP.2016.2577003.

[52] S. X. Ta, N. Nguyen-Trong, V. C. Nguyen, K. K. Nguyen, and C. Dao-Ngoc, "Broadband Dual-Polarized Antenna Using Metasurface for Full-Duplex Applications," *IEEE Antennas and Wireless Propagation Letters*, vol. 20, no. 2, pp. 254–258, Feb. 2021, doi: 10.1109/LAWP.2020.3047231.

[53] S. G. Kirtania *et al.*, "Flexible Antennas: A Review," *Micromachines*, vol. 11, no. 9, Art. no. 9, Sep. 2020, doi: 10.3390/mi11090847.

[54] A. W. Memon, I. L. de Paula, B. Malengier, S. Vasile, P. Van Torre, and L. Van Langenhove, "Breathable Textile Rectangular Ring Microstrip Patch Antenna at 2.45 GHz for Wearable Applications," *Sensors*, vol. 21, no. 5, Art. no. 5, Jan. 2021, doi: 10.3390/s21051635.

[55] M. I. Ahmed, M. F. Ahmed, and A.-E. H. Shaalan, "Novel electro-textile patch antenna on jeans substrate for wearable applications," *PIER C*, vol. 83, pp. 255–265, 2018, doi: 10.2528/PIERC18030309.

[56] F. Nikbakhtnasrabadi, H. El Matbouly, M. Ntagios, and R. Dahiya, "Textile-Based Stretchable Microstrip Antenna with Intrinsic Strain Sensing," *ACS Appl. Electron. Mater.*, vol. 3, no. 5, pp. 2233–2246, May 2021, doi: 10.1021/acsaelm.1c00179.

[57] S. G. Kirtania, B. A. Younes, A. R. Hossain, T. Karacolak, and P. K. Sekhar, "CPW-Fed Flexible Ultra-Wideband Antenna for IoT Applications," *Micromachines*, vol. 12, no. 4, Art. no. 4, Apr. 2021, doi: 10.3390/mi12040453.

[58] M. F. Farooqui and A. Kishk, "3-D-Printed Tunable Circularly Polarized Microstrip Patch Antenna," *IEEE Antennas and Wireless Propagation Letters*, vol. 18, no. 7, pp. 1429–1432, Jul. 2019, doi: 10.1109/LAWP.2019.2919255.

[59] H. F. Abutarboush, W. Li, and A. Shamim, "Flexible-Screen-Printed Antenna With Enhanced Bandwidth by Employing Defected Ground Structure," *IEEE Antennas and Wireless Propagation Letters*, vol. 19, no. 10, pp. 1803–1807, Oct. 2020, doi: 10.1109/LAWP.2020.3019462.

[60] N. A. Tran, H. N. Tran, M. C. Dang, and E. Fribourg-Blanc, "Copper thin film for RFID UHF antenna on flexible substrate," *Adv. Nat. Sci: Nanosci. Nanotechnol.*, vol. 1, no. 2, p. 025016, Aug. 2010, doi: 10.1088/2043-6254/1/2/025016.

[61] O. E. Maleky, F. B. Abdelouahab, M. Essaaidi, and M. Ali. Ennasar, "Design of simple printed Dipole antenna on flexible substrate for UHF band," *Procedia Manufacturing*, vol. 22, pp. 428–435, Jan. 2018, doi: 10.1016/j.promfg.2018.03.067.

[62] S. J. Chen, C. Fumeaux, B. Chivers, and R. Shepherd, "A 5.8-GHz flexible microstrip-fed slot antenna realized in PEDOT:PSS conductive polymer," in *2016 IEEE International Symposium on Antennas and Propagation (APSURSI)*, Jun. 2016, pp. 1317–1318. doi: 10.1109/APS.2016.7696366.

[63] M. Kadry, M. E. Atrash, and Mahmoud. A. Abdalla, “Design of an Ultra-thin Compact Flexible Dual-Band Antenna for Wearable Applications,” in *2018 IEEE International Symposium on Antennas and Propagation & USNC/URSI National Radio Science Meeting*, Jul. 2018, pp. 1949–1950. doi: 10.1109/APUSNCURSINRSM.2018.8609247.

[64] M. E. Jalil, M. K. A. Rahim, N. A. Samsuri, N. A. Murad, N. Othman, and H. A. Majid, “On-body investigation of dual band diamond textile antenna for wearable applications at 2.45 GHz and 5.8 GHz,” in *2013 7th European Conference on Antennas and Propagation (EuCAP)*, Apr. 2013, pp. 414–417.

[65] Z. Hamouda, J. Wojkiewicz, A. A. Pud, L. Kone, S. Bergheul, and T. Lasri, “Flexible UWB organic antenna for wearable technologies application,” *IET Microwaves, Antennas & Propagation*, vol. 12, no. 2, pp. 160–166, 2018, doi: 10.1049/iet-map.2017.0189.

[66] C.-Z. Du, K.-J. Li, and S.-S. Zhong, “A novel flexible hexagon wideband CPW-fed monopole antenna for UWB applications,” *Microwave and Optical Technology Letters*, vol. 63, no. 7, pp. 1899–1905, 2021, doi: 10.1002/mop.32832.

[67] C. X. Mao, Y. Zhou, Y. Wu, H. Soewardiman, D. H. Werner, and J. S. Jur, “Low-Profile Strip-Loaded Textile Antenna With Enhanced Bandwidth and Isolation for Full-Duplex Wearable Applications,” *IEEE Transactions on Antennas and Propagation*, vol. 68, no. 9, pp. 6527–6537, Sep. 2020, doi: 10.1109/TAP.2020.2989862.

[68] M. Wagih, G. S. Hilton, A. S. Weddell, and S. Beeby, “Dual-Polarized Wearable Antenna/Rectenna for Full-Duplex and MIMO Simultaneous Wireless Information and Power Transfer (SWIPT),” *IEEE Open Journal of Antennas and Propagation*, vol. 2, pp. 844–857, 2021, doi: 10.1109/OJAP.2021.3098939.

[69] C.-X. Mao, D. Vital, D. H. Werner, Y. Wu, and S. Bhardwaj, “Dual-Polarized Embroidered Textile Armband Antenna Array With Omnidirectional Radiation for On-/Off-Body Wearable Applications,” *IEEE Transactions on Antennas and Propagation*, vol. 68, no. 4, pp. 2575–2584, Apr. 2020, doi: 10.1109/TAP.2019.2951517.

[70] N. K. Mallat and A. Iqbal, “Substrate integrated waveguide-based simultaneous transmit and receive antenna for full-duplex wearable devices,” *International Journal of RF and Microwave Computer-Aided Engineering*, vol. 32, no. 7, p. e23188, 2022, doi: 10.1002/mmce.23188.

[71] D. Guha, M. Biswas, and Y. M. M. Antar, “Microstrip Patch Antenna With Defected Ground Structure for Cross Polarization Suppression,” *IEEE Antennas and Wireless Propagation Letters*, vol. 4, pp. 455–458, 2005, doi: 10.1109/LAWP.2005.860211.

[72] Y. J. Sung, M. Kim, and Y. S. Kim, “Harmonics reduction with defected ground structure for a microstrip patch antenna,” *IEEE Antennas and Wireless Propagation Letters*, vol. 2, pp. 111–113, 2003, doi: 10.1109/LAWP.2003.815281.

[73] K. H. Chiang and K. W. Tam, “Microstrip Monopole Antenna With Enhanced Bandwidth Using Defected Ground Structure,” *IEEE Antennas and Wireless Propagation Letters*, vol. 7, pp. 532–535, 2008, doi: 10.1109/LAWP.2008.2005592.

[74] Y. Chung, S.-S. Jeon, D. Ahn, J.-I. Choi, and T. Itoh, “High isolation dual-polarized patch antenna using integrated defected ground structure,” *IEEE Microwave and Wireless Components Letters*, vol. 14, no. 1, pp. 4–6, Jan. 2004, doi: 10.1109/LMWC.2003.821501.

[75] C. Kumar, M. I. Pasha, and D. Guha, “Defected Ground Structure Integrated Microstrip Array Antenna for Improved Radiation Properties,” *IEEE Antennas and Wireless Propagation Letters*, vol. 16, pp. 310–312, 2017, doi: 10.1109/LAWP.2016.2574638.

[76] L. H. Weng, Y.-C. Guo, X.-W. Shi, and X.-Q. Chen, “An overview on defected ground structure,” *PIER B*, vol. 7, pp. 173–189, 2008, doi: 10.2528/PIERB08031401.

[77] H. Yang, X. Liu, Y. Fan, and L. Xiong, “Dual-Band Textile Antenna With Dual Circular Polarizations Using Polarization Rotation AMC for Off-Body Communications,” *IEEE Transactions on Antennas and Propagation*, vol. 70, no. 6, pp. 4189–4199, Jun. 2022, doi: 10.1109/TAP.2021.3138504.

[78] S. Doddipalli, A. Kothari, and P. Peshwe, “A Low Profile Ultrawide Band Monopole Antenna for Wearable Applications,” *International Journal of Antennas and Propagation*, vol. 2017, p. e7362431, Aug. 2017, doi: 10.1155/2017/7362431.

[79] B. Almohammed, A. Ismail, and A. Sali, “Electro-textile wearable antennas in wireless body area networks: materials, antenna design, manufacturing techniques, and human body consideration—a review,” *Textile Research Journal*, vol. 91, no. 5–6, pp. 646–663, Mar. 2021, doi: 10.1177/0040517520932230.

[80] D. Wen, Y. Hao, M. O. Munoz, H. Wang, and H. Zhou, "A Compact and Low-Profile MIMO Antenna Using a Miniature Circular High-Impedance Surface for Wearable Applications," *IEEE Transactions on Antennas and Propagation*, vol. 66, no. 1, pp. 96–104, Jan. 2018, doi: 10.1109/TAP.2017.2773465.

[81] A. T. Castro and S. K. Sharma, "Inkjet-Printed Wideband Circularly Polarized Microstrip Patch Array Antenna on a PET Film Flexible Substrate Material," *IEEE Antennas and Wireless Propagation Letters*, vol. 17, no. 1, pp. 176–179, Jan. 2018, doi: 10.1109/LAWP.2017.2779440.

[82] A. M. Ali, M. El Atrash, S. R. Zahran, and M. A. Abdalla, "A Low Profile Flexible Circularly Polarized Antenna for Wearable and WLAN Applications," in *2019 IEEE International Symposium on Antennas and Propagation and USNC-URSI Radio Science Meeting*, Jul. 2019, pp. 1603–1604. doi: 10.1109/APUSNCURSINRSM.2019.8889131.

[83] Md. R. Hasan, M. A. Riheen, P. Sekhar, and T. Karacolak, "Compact CPW-fed circular patch flexible antenna for super-wideband applications," *IET Microwaves, Antennas & Propagation*, vol. 14, no. 10, pp. 1069–1073, 2020, doi: 10.1049/iet-map.2020.0155.

[84] S. Moscato *et al.*, "Infill-Dependent 3-D-Printed Material Based on NinjaFlex Filament for Antenna Applications," *IEEE Antennas and Wireless Propagation Letters*, vol. 15, pp. 1506–1509, 2016, doi: 10.1109/LAWP.2016.2516101.

[85] M. E. Lajevardi and M. Kamyab, "Ultraminiaturized Metamaterial-Inspired SIW Textile Antenna for Off-Body Applications," *IEEE Antennas and Wireless Propagation Letters*, vol. 16, pp. 3155–3158, 2017, doi: 10.1109/LAWP.2017.2766201.

[86] Y. Wang *et al.*, "A facile process combined with roll-to-roll flexographic printing and electroless deposition to fabricate RFID tag antenna on paper substrates," *Composites Part B: Engineering*, vol. 224, p. 109194, Nov. 2021, doi: 10.1016/j.compositesb.2021.109194.

[87] M. A. Riheen, T. T. Nguyen, T. K. Saha, T. Karacolak, and P. K. Sekhar, "Cpw fed wideband bowtie slot antenna on pet substrate," *PIER C*, vol. 101, pp. 147–158, 2020, doi: 10.2528/PIERC20031402.

[88] U. Ullah, I. B. Mabrouk, and S. Koziel, "A Compact Circularly Polarized Antenna With Directional Pattern for Wearable Off-Body Communications," *IEEE Antennas and Wireless Propagation Letters*, vol. 18, no. 12, pp. 2523–2527, Dec. 2019, doi: 10.1109/LAWP.2019.2942147.

[89] K. Fujita, K. Yoshitomi, K. Yoshida, and H. Kanaya, “A circularly polarized planar antenna on flexible substrate for ultra-wideband high-band applications,” *AEU - International Journal of Electronics and Communications*, vol. 69, no. 9, pp. 1381–1386, Sep. 2015, doi: 10.1016/j.aeue.2015.06.005.

[90] H.-R. Zu, B. Wu, Y.-H. Zhang, Y.-T. Zhao, R.-G. Song, and D.-P. He, “Circularly Polarized Wearable Antenna With Low Profile and Low Specific Absorption Rate Using Highly Conductive Graphene Film,” *IEEE Antennas and Wireless Propagation Letters*, vol. 19, no. 12, pp. 2354–2358, Dec. 2020, doi: 10.1109/LAWP.2020.3033013.

[91] Y. Chen, X. Liu, Y. Fan, and H. Yang, “Wearable Wideband Circularly Polarized Array Antenna for Off-Body Applications,” *IEEE Antennas and Wireless Propagation Letters*, vol. 21, no. 5, pp. 1051–1055, May 2022, doi: 10.1109/LAWP.2022.3157367.